

# Novel Higgs-to-125 GeV Higgs boson decays in the complex NMSSM

Shoaib Munir\*

National Centre for Nuclear Research, Hoza 69, 00-681 Warsaw, Poland

April 4, 2024

## Abstract

In the Next-to-Minimal Supersymmetric Standard Model (NMSSM) a variety of parameter configurations yields a Higgs boson consistent with the one observed at the LHC. Additionally, the Higgs sector of the model can contain explicit CP-violating phases even at the tree level, in contrast with the Minimal Supersymmetric Standard Model (MSSM). In this article we present the one-loop Higgs boson mass matrix of the complex NMSSM in the renormalisation-group-improved effective potential approach. We also present the trilinear Higgs boson self-couplings as well as various partial decay widths of a generic CP-mixed Higgs boson in the model. We then analyse a very interesting phenomenological scenario wherein the decay of a relatively light pseudoscalar-like Higgs boson into  $\sim 125$  GeV SM-like Higgs boson(s) is induced by non-zero CP-violating phases. We discuss in detail a few benchmark cases in which such a decay can contribute significantly to the production of SM-like Higgs bosons at the LHC on top of the gluon fusion process. It can thus be partially responsible for the  $\gamma\gamma$  excess near 125 GeV due to the subsequent decay of the SM-like Higgs boson. Such a scenario is extremely difficult to realize in the complex MSSM and, if probed at the LHC, it could provide an indication of the non-minimal nature of supersymmetry.

## 1 Introduction

The new particle with mass around 125 GeV first observed by the CMS and ATLAS experimental collaborations at the Large Hadron Collider (LHC) in July 2012 [1, 2] seems to be increasingly consistent with the Higgs boson of the Standard Model (SM) [3, 4, 5]. However, there is growing evidence from other collider experiments as well as from astroparticle physics and cosmology that the SM fails to provide a complete description of nature and that there must lie physics beyond it. One of the most important yet unresolved issues in particle physics is that of CP violation. Although it was first discovered experimentally [6] many decades ago, its only source in the SM [7] does not prove sufficient to explain the observed baryon asymmetry in the Universe. Therefore, a variety of sources of CP violation beyond the SM have been proposed in the literature (for a review, see [8] and references therein), but these remain hidden to this day.

In models with supersymmetry (SUSY), the soft masses and couplings of the superpartners of SM particles as well as the soft Higgs sector parameters can very well be complex and can thus explain baryogenesis by generating the desired amount of CP-violation. The Higgs sector of the

---

\*Present address: Department of Physics and Astronomy, Uppsala University, Box 516, SE-751 20 Uppsala, Sweden.

email: shoaib.munir@physics.uu.se

Minimal Supersymmetric Standard Model (MSSM) does not contain CP-violating (CPV) phases at the tree level and these are only induced at the one-loop level by the sfermion sector [9, 10, 11]. These phases can substantially modify both the mass spectrum and production/decay rates of the Higgs bosons [12] and can at the same time provide a solution to electroweak baryogenesis [13]. However, these phases are also strongly constrained by the measurements of fermionic electric dipole moments (EDMs) [14]. In the context of the LHC, the impact of the CPV phases on the phenomenology of the MSSM Higgs bosons was studied in detail in [15] prior to the Higgs boson discovery and has been revisited in [16] afterwards.

In the Next-to-Minimal Supersymmetric Standard Model (NMSSM) [17, 18, 19] (see, e.g., [20, 21] for reviews) the presence of an additional Higgs singlet field besides the two MSSM doublets has some very interesting phenomenological implications. In this model either of the two lightest CP-even Higgs bosons,  $h_1$  and  $h_2$ , can play the role of the observed SM-like Higgs boson with a mass around 125 GeV [22]. In fact in the NMSSM it is also possible to have  $h_1$  and  $h_2$  almost degenerate in mass around 125 GeV [23], so that the observed signal is actually a superposition of two individual peaks due to each of these, and likewise for  $h_1$  and  $a_1$ , the lightest pseudoscalar of the model [24]. Additionally, in some regions of the NMSSM parameter space the singlet-like scalar or pseudoscalar of the model can be considerably lighter than the SM-like Higgs boson. In these regions the SM-like Higgs boson can decay via such ‘invisible’ channels, causing a significant suppression of the  $\gamma\gamma$  and  $ZZ$  signal rates, as studied recently in [25, 26].

The NMSSM contains some new couplings in the Higgs sector which, if assumed to be complex, can result in new CPV phases even at the tree level, conversely to the MSSM. Indeed, additional MSSM-like phases also appear in the Higgs boson mass matrix beyond the born approximation. Non-zero CPV phases can substantially modify the phenomenology of the  $\sim 125$  GeV SM-like Higgs boson in the NMSSM, as studied recently in [27]. But, like the MSSM, the measurements of fermionic EDMs can put strong constraints on the allowed values of the CPV phases in the NMSSM also. However, the conditions under which these EDM constraints can be avoided in the MSSM [10, 28] in fact also apply in this model. One can, for example, assign very heavy soft masses to the sfermions of the first two generations in order to minimize their contribution to the EDMs. Alternatively, one can argue that the phase combinations occurring in the EDMs can be different from the ones inducing Higgs boson mixing [29].

The complete one-loop Higgs mass matrix has been derived in [30] in the Feynman diagrammatic approach. In the renormalisation-group (RG)-improved effective potential approach the neutral Higgs sector of the complex NMSSM (cNMSSM) has previously been studied in detail in [31, 32], including only the dominant one-loop corrections from the (s)quark and gauge sectors. In this article, we provide the RG-improved one-loop Higgs mass matrix of the cNMSSM in the effective potential approach in which the complete set of dominant corrections from the third generation (s)quark, stau, gauge as well as chargino/neutralino sectors have been included. We also present the tree level expression for the trilinear Higgs boson self-couplings in the cNMSSM. These couplings are extremely important for studying the LHC phenomenology of Higgs bosons in the model. Moreover, we present the set of expressions for partial decay widths of a CPV Higgs boson.

The Higgs boson mass matrix and decay widths provided here have been implemented in a comprehensive fortran package for conveniently carrying out phenomenological studies of the cNMSSM Higgs sector. Using this package we analyse in this article a very interesting scenario made possible by non-zero CPV phases in the NMSSM, owing to the fact that the five neutral Higgs bosons of the model no longer carry definite CP assignments. The scalars and pseudoscalars of the CP-conserving (CPC) limit thus couple to one another, which implies that any of these Higgs bosons can have a non-zero decay width into a pair of lighter ones, when kinematically allowed. We argue that such a scenario can be of particular importance in the context of the recent LHC

discovery. The reason is that it is very much probable for the lighter of the two pseudoscalar-like Higgs bosons to have a mass  $\sim 250$  GeV, particularly when one of the scalar-like Higgs bosons is required to have SM-like  $\gamma\gamma$  and  $ZZ$  signal rates and a mass near 125 GeV. Such a mass would result a much larger branching ratio (BR) of this Higgs boson into a pair of the SM-like Higgs bosons compared to that of the other, typically much heavier, scalar-like Higgs bosons, despite a relatively much smaller trilinear coupling.

However, despite having a large BR into lighter Higgs bosons, the above mentioned  $\sim 250$  GeV boson can be very difficult to produce at the LHC on account of being singlet-like and thus having a considerably reduced coupling to two gluons. Therefore, the relative probability of its production in the gluon fusion mode also needs to be taken into account in the above scenario. For this purpose, we define an auxiliary signal rate, similar to the conventional ‘reduced cross section’, which quantifies the contribution of the  $\sim 250$  GeV boson to the production of the SM-like Higgs bosons, decaying eventually into photons pairs, at the LHC. We then select representative points from three distinct regions in the cNMSSM parameter space wherein the  $\sim 125$  GeV SM-like Higgs boson is either  $h_1$  or  $h_2$ , the lightest and next-to-lightest of the five neutral Higgs bosons, respectively, to investigate our scenario of interest. We discuss in detail the impact of the variation in the most relevant of the CPV phases on our auxiliary signal rate in each of these cases. We conclude that for large values of the phase, this rate can become quite significant, reaching a few tens of percent of the direct production rate of the SM-like Higgs boson in the gluon fusion channel.

The article is organised as follows. In the next section we will give details of the cNMSSM Higgs mass matrix at the tree level and the one-loop as well as logarithmically enhanced dominant two-loop corrections to it. In Sect. 3 we will present the expressions for the trilinear self-couplings of the Higgs bosons and will also define notation for their couplings to other model particles. In Sect. 4 we will provide detailed expressions for all possible two-body partial decay widths of the Higgs boson in the presence of CPV phases. In Sect. 5, after discussing at length our scenario of interest, we will present our numerical results for the three points investigated. We will summarise our findings in Sect. 6.

## 2 Higgs sector of the cNMSSM

As noted in the introduction, the NMSSM contains a singlet Higgs superfield,  $\hat{S}$ , besides the two MSSM  $SU(2)_L$  doublet superfields,

$$\hat{H}_u = \begin{pmatrix} \hat{H}_u^+ \\ \hat{H}_u^0 \end{pmatrix}, \quad \hat{H}_d = \begin{pmatrix} \hat{H}_d^0 \\ \hat{H}_d^- \end{pmatrix}. \quad (1)$$

The scale-invariant superpotential of the cNMSSM is thus written as

$$W_{\text{NMSSM}} = \text{MSSM Yukawa terms} + \lambda \hat{S} \hat{H}_u \hat{H}_d + \frac{\kappa}{3} \hat{S}^3, \quad (2)$$

where  $\lambda \equiv |\lambda|e^{i\phi_\lambda}$  and  $\kappa \equiv |\kappa|e^{i\phi_\kappa}$  are dimensionless complex Yukawa couplings. The second term in the above superpotential replaces the Higgs-higgsino mass term,  $\mu \hat{H}_u \hat{H}_d$ , of the MSSM superpotential and the last cubic term explicitly breaks the dangerous  $U(1)_{PQ}$  symmetry, introducing in turn a discrete  $Z_3$  symmetry. Upon breaking the electroweak symmetry, the singlet field acquires a vacuum expectation value (Vev),  $s$ , naturally of the order of the SUSY-breaking scale,  $M_{\text{SUSY}}$ , and an effective  $\mu$ -term,  $\mu_{\text{eff}} = \lambda s$ , is generated.

## 2.1 Tree level Higgs potential and mass matrix

The superpotential in Eq. (2) leads to the tree level Higgs potential containing the  $D$ -,  $F$ - and soft SUSY-breaking terms:

$$\begin{aligned}
V_0 = & \left| \lambda (H_u^+ H_d^- - H_u^0 H_d^0) + \kappa S^2 \right|^2 \\
& + \left( m_{H_u}^2 + |\mu + \lambda S|^2 \right) \left( |H_u^0|^2 + |H_u^+|^2 \right) + \left( m_{H_d}^2 + |\mu + \lambda S|^2 \right) \left( |H_d^0|^2 + |H_d^-|^2 \right) \\
& + \frac{g^2}{4} \left( |H_u^0|^2 + |H_u^+|^2 - |H_d^0|^2 - |H_d^-|^2 \right)^2 + \frac{g_2^2}{2} |H_u^+ H_d^{0*} + H_u^0 H_d^{-*}|^2 \\
& + m_S^2 |S|^2 + (\lambda A_\lambda (H_u^+ H_d^- - H_u^0 H_d^0) S + \frac{1}{3} \kappa A_\kappa S^3 + \text{h.c.}), \tag{3}
\end{aligned}$$

where  $g^2 \equiv \frac{g_1^2 + g_2^2}{2}$ , with  $g_1$  and  $g_2$  being the  $U(1)_Y$  and  $SU(2)_L$  gauge couplings, respectively, and  $A_\lambda \equiv |A_\lambda| e^{i\phi_{A_\lambda}}$  and  $A_\kappa \equiv |A_\kappa| e^{i\phi_{A_\kappa}}$  are dimensionful soft SUSY-breaking trilinear couplings. These, along with  $\lambda$  and  $\kappa$ , are the only complex parameters appearing in the tree level Higgs potential, since the soft SUSY-breaking masses  $m_{H_u}^2$ ,  $m_{H_d}^2$  and  $m_{H_u}^2$  are real.

In order to obtain the physical Higgs states, the above potential is expanded around the VEVs of the three Higgs fields as

$$\begin{aligned}
H_d^0 &= \begin{pmatrix} \frac{1}{\sqrt{2}} (v_d + H_{dR} + iH_{dI}) \\ H_d^- \end{pmatrix}, \\
H_u^0 &= e^{i\theta} \begin{pmatrix} H_u^+ \\ \frac{1}{\sqrt{2}} (v_u + H_{uR} + iH_{uI}) \end{pmatrix}, \\
S &= \frac{e^{i\varphi}}{\sqrt{2}} (s + S_R + iS_I). \tag{4}
\end{aligned}$$

The potential in Eq. (3) then has a minimum at non-vanishing  $v_u$ ,  $v_d$  and  $s$  only if the following so-called tadpole conditions are satisfied:

$$\begin{aligned}
\frac{1}{v_d} \left\langle \frac{\partial V_0}{\partial H_{dR}} \right\rangle &= m_{H_d}^2 + \frac{g^2}{4} (v_d^2 - v_u^2) - R_\lambda \frac{v_u s}{v_d} + \frac{|\lambda|^2}{2} (v_u^2 + s^2) - \frac{1}{2} \mathcal{R} \frac{v_u s^2}{v_d} = 0, \\
\frac{1}{v_u} \left\langle \frac{\partial V_0}{\partial H_{uR}} \right\rangle &= m_{H_u}^2 - \frac{g^2}{4} (v_d^2 - v_u^2) - R_\lambda \frac{v_d s}{v_u} + \frac{|\lambda|^2}{2} (v_d^2 + s^2) - \frac{1}{2} \mathcal{R} \frac{v_d s^2}{v_u} = 0, \\
\frac{1}{s} \left\langle \frac{\partial V_0}{\partial S_R} \right\rangle &= m_S^2 - R_\lambda \frac{v_d v_u}{s} + \frac{|\lambda|^2}{2} (v_d^2 + v_u^2) + |\kappa|^2 s^2 - \mathcal{R} v_d v_u + R_\kappa s = 0, \tag{5}
\end{aligned}$$

$$\begin{aligned}
\frac{1}{v_u} \left\langle \frac{\partial V_0}{\partial H_{dI}} \right\rangle &= \frac{1}{v_d} \left\langle \frac{\partial V_0}{\partial H_{uI}} \right\rangle = I_\lambda s + \frac{1}{2} \mathcal{I} s^2 = 0, \\
\frac{1}{s} \left\langle \frac{\partial V_0}{\partial S_I} \right\rangle &= I_\lambda \frac{v_d v_u}{s} - \mathcal{I} v_d v_u - I_\kappa s = 0, \tag{6}
\end{aligned}$$

where we have defined

$$\begin{aligned}
\mathcal{R} &= |\lambda| |\kappa| \cos(\phi'_\lambda - \phi'_\kappa), & \mathcal{I} &= |\lambda| |\kappa| \sin(\phi'_\lambda - \phi'_\kappa), \\
R_\lambda &= \frac{|\lambda| |A_\lambda|}{\sqrt{2}} \cos(\phi'_\lambda + \phi_{A_\lambda}), & R_\kappa &= \frac{|\kappa| |A_\kappa|}{\sqrt{2}} \cos(\phi'_\kappa + \phi_{A_\kappa}), \\
I_\lambda &= \frac{|\lambda| |A_\lambda|}{\sqrt{2}} \sin(\phi'_\lambda + \phi_{A_\lambda}), & I_\kappa &= \frac{|\kappa| |A_\kappa|}{\sqrt{2}} \sin(\phi'_\kappa + \phi_{A_\kappa}), \tag{7}
\end{aligned}$$

with

$$\phi'_\lambda \equiv \phi_\lambda + \theta + \varphi \quad \text{and} \quad \phi'_\kappa \equiv \phi_\kappa + 3\varphi. \quad (8)$$

The parameters  $I_\lambda$  and  $I_\kappa$  can be re-expressed in terms of  $\mathcal{I}$  using the CP-odd tadpole conditions in Eq. (6) as

$$I_\lambda = -\frac{1}{2}\mathcal{I}s, \quad I_\kappa = -\frac{3}{2}\mathcal{I}\frac{v_d v_u}{s}. \quad (9)$$

Then the phase combinations  $\phi'_\lambda + \phi_{A_\lambda}$  and  $\phi'_\kappa + \phi_{A_\kappa}$  are determined up to a twofold ambiguity by  $\phi'_\lambda - \phi'_\kappa$ , which is thus the only remaining physical CP phase at the tree level. The three CP-even tadpole conditions in Eq. (5), on the other hand, can be used to remove the soft mass parameters  $m_{H_u}^2$ ,  $m_{H_d}^2$  and  $m_S^2$ .

The  $6 \times 6$  neutral Higgs mass matrix, obtained by taking the second derivative of the potential in Eq. (3) evaluated at the vacuum, can be cast into the form

$$\mathcal{M}_0^2 = \begin{pmatrix} \mathcal{M}_S^2 & \mathcal{M}_{SP}^2 \\ (\mathcal{M}_{SP}^2)^T & \mathcal{M}_P^2 \end{pmatrix}, \quad (10)$$

in the basis  $\mathbf{H}^T = (H_{dR}, H_{uR}, S_R, H_{dI}, H_{uI}, S_I)$ . The elements of the top left  $3 \times 3$  CP-even block in the above equation are given as

$$\begin{aligned} \mathcal{M}_{S,11}^2 &= \frac{g^2}{2}v_d^2(Q) + \left(R_\lambda + \frac{\mathcal{R}s(Q)}{2}\right)s(Q)\tan\beta, \\ \mathcal{M}_{S,22}^2 &= \frac{g^2}{2}v_u^2(Q) + \left(R_\lambda + \frac{\mathcal{R}s(Q)}{2}\right)\frac{s(Q)}{\tan\beta}, \\ \mathcal{M}_{S,33}^2 &= R_\lambda\frac{v_d(Q)v_u(Q)}{s(Q)} + 2|\kappa|^2s(Q)^2 + R_\kappa s(Q), \\ \mathcal{M}_{S,12}^2 &= (\mathcal{M}_{S,21}^2) = \left(-\frac{g_1^2 + g_2^2}{4} + |\lambda|^2\right)v_d(Q)v_u(Q) - \left(R_\lambda + \frac{\mathcal{R}s(Q)}{2}\right)s(Q), \\ \mathcal{M}_{S,13}^2 &= (\mathcal{M}_{S,31}^2) = -R_\lambda v_u(Q) + |\lambda|^2 v_d(Q)s(Q) - \mathcal{R}v_u(Q)s(Q), \\ \mathcal{M}_{S,23}^2 &= (\mathcal{M}_{S,32}^2) = -R_\lambda v_d(Q) + |\lambda|^2 v_u(Q)s(Q) - \mathcal{R}v_d(Q)s(Q), \end{aligned} \quad (11)$$

where  $v_u(Q)$ ,  $v_d(Q)$  and  $s(Q)$  are the three Higgs VEVs defined at the scale  $Q^2 = M_{\text{SUSY}}^2$  and  $\tan\beta \equiv v_u(Q)/v_d(Q)$ . The bottom right CP-odd block in Eq. (10) is given as

$$\begin{aligned} \mathcal{M}_{P,11}^2 &= \left(R_\lambda + \frac{\mathcal{R}s(Q)}{2}\right)s(Q)\tan\beta, \\ \mathcal{M}_{P,22}^2 &= \left(R_\lambda + \frac{\mathcal{R}s(Q)}{2}\right)\frac{s(Q)}{\tan\beta}, \\ \mathcal{M}_{P,33}^2 &= R_\lambda\frac{v_d(Q)v_u(Q)}{s(Q)} + 2\mathcal{R}v_d(Q)v_u(Q) - 3R_\kappa s(Q), \\ \mathcal{M}_{P,12}^2 &= (\mathcal{M}_{P,21}^2) = \left(R_\lambda + \frac{\mathcal{R}s(Q)}{2}\right)s(Q), \\ \mathcal{M}_{S,13}^2 &= (\mathcal{M}_{S,31}^2) = (R_\lambda - \mathcal{R}s(Q))v_u(Q), \\ \mathcal{M}_{S,23}^2 &= (\mathcal{M}_{S,32}^2) = (R_\lambda - \mathcal{R}s(Q))v_d(Q), \end{aligned} \quad (12)$$

and the off-diagonal CP-mixing block reads

$$\mathcal{M}_{SP}^2 = \begin{pmatrix} 0 & 0 & -\frac{3}{2}\mathcal{I}s v_u \\ 0 & 0 & -\frac{3}{2}\mathcal{I}s v_d \\ \frac{1}{2}\mathcal{I}s v_u & \frac{1}{2}\mathcal{I}s v_d & 2\mathcal{I}v_d v_u \end{pmatrix}. \quad (13)$$

## 2.2 RG-improved one-loop effective potential

The one-loop corrections to the effective potential are given by the Coleman-Weinberg formula (in the  $\overline{\text{DR}}$  scheme with an ultraviolet cutoff  $M_{\text{SUSY}}^2$ ) as

$$\Delta V_{\text{eff}} = \frac{1}{64\pi^2} \text{STr } M^4 \left[ \ln \left( \frac{M^2}{M_{\text{SUSY}}^2} \right) - \frac{3}{2} \right]. \quad (14)$$

As a result of these corrections the Higgs mass matrix gets modified so that

$$\mathcal{M}_H^2 = \mathcal{M}_0^2 + \Delta \mathcal{M}_{\text{eff}}^2. \quad (15)$$

In the following we present analytical expressions for the corrections  $\Delta \mathcal{M}_{\text{eff}}^2$  above. These corrections have been adopted from [20] and modified to explicitly include the CPV phases. They are thus of the same order as those implemented in the publicly available package NMSSMTools-v3.2.4 [33].

### 2.2.1 Top and bottom squark contributions

Some of the radiative corrections due to the stop and sbottom loops can be accounted for by the following shift in the Higgs mass matrix:

$$A_\lambda \rightarrow A'_\lambda = A_\lambda + \frac{3h_t^2}{16\pi^2} A_t f_t + \frac{3h_b^2}{16\pi^2} A_b f_b, \quad (16)$$

where  $h_t \equiv \frac{2m_t}{v_u}$  and  $h_b \equiv \frac{2m_b}{v_d}$  are the Yukawa couplings of top and bottom quarks, with  $m_t$  and  $m_b$  being their respective masses. Note that these Yukawa couplings have complex phases in general. However, we assume them to be real, since their non-zero phases can always be reabsorbed by redefining the quark fields [7] when generation mixing is neglected, which is the case here.  $A_t \equiv |A_t|e^{i\phi_{A_t}}$  and  $A_b \equiv |A_b|e^{i\phi_{A_b}}$  are the complex soft SUSY-breaking counterparts of these Yukawa couplings for the top and bottom squarks, respectively.

The above shift results in the redefinition of the parameters  $\mathcal{R}$  and  $\mathcal{I}$  given in Eq. (7) and a subsequent improvement in the relation between the latter and  $I_\lambda$  given in Eq. (9). It also takes care of the  $\sim h_{t,b}^4$  radiative corrections to  $\mathcal{M}_P^2$ . The remaining corrections  $\sim h_t^2 \equiv h_t^2(M_{\text{SUSY}}^2)$  and  $\sim h_b^2 \equiv h_b^2(M_{\text{SUSY}}^2)$  to  $\mathcal{M}_S^2$  are written as

$$\begin{aligned} \Delta \mathcal{M}_{S,11}^2 &= \frac{3h_b^2 m_b^2}{8\pi^2} \left( -|A_b|^2 B'_b g_b + 2|A_b| B_b L_{\bar{b}} + L_{\bar{b}b} \right) - \frac{3h_t^2 m_t^2}{8\pi^2} |\mu|^2 B'_t g_t, \\ \Delta \mathcal{M}_{S,22}^2 &= \frac{3h_t^2 m_t^2}{8\pi^2} \left( -|A_t|^2 B'_t g_t + 2|A_t| B_t L_{\bar{t}} + L_{\bar{t}t} \right) - \frac{3h_b^2 m_b^2}{8\pi^2} |\mu|^2 B'_b g_b, \\ \Delta \mathcal{M}_{S,33}^2 &= -\frac{3h_t^2 m_t^2}{16\pi^2} |\lambda|^2 v_d^2(Q) B'_t g_t - \frac{3h_b^2 m_b^2}{16\pi^2} |\lambda|^2 v_u^2(Q) B'_b g_b, \\ \Delta \mathcal{M}_{S,12}^2 &= \frac{3h_t^2 m_t^2}{8\pi^2} |\mu| \left( |A_t| B'_t g_t \cos(\phi'_\lambda + \phi_{A_t}) - \frac{|A_t| \cos(\phi'_\lambda + \phi_{A_t}) + |\mu| \cot \beta}{m_{\tilde{t}_2^2} - m_{\tilde{t}_1^2}} \right) \\ &\quad + \frac{3h_b^2 m_b^2}{8\pi^2} |\mu| \left( |A_b| B'_b g_b \cos(\phi'_\lambda + \phi_{A_b}) - \frac{|A_b| \cos(\phi'_\lambda + \phi_{A_b}) + |\mu| \tan \beta}{m_{\tilde{b}_2^2} - m_{\tilde{b}_1^2}} \right), \\ \Delta \mathcal{M}_{S,13}^2 &= \frac{3h_b^2 m_b^2 |\lambda| v_u(Q)}{8\sqrt{2}\pi^2} \left( |A_b| B'_b g_b \cos(\phi'_\lambda + \phi_{A_b}) - \frac{|A_b| \cos(\phi'_\lambda + \phi_{A_b}) + |\mu| \tan \beta}{m_{\tilde{b}_2^2} - m_{\tilde{b}_1^2}} \right) \\ &\quad + \frac{3h_t^2}{64\pi^2} |\lambda|^2 s(Q) v_d(Q) (4f_t - 4m_t^2 B'_t g_t), \end{aligned}$$

$$\begin{aligned}\Delta\mathcal{M}_{S,23}^2 &= \frac{3h_t^2 m_t^2 |\lambda| v_d(Q)}{8\sqrt{2}\pi^2} \left( |A_t| B'_t g_t \cos(\phi'_\lambda + \phi_{A_t}) - \frac{|A_t| \cos(\phi'_\lambda + \phi_{A_t}) + |\mu| \cot \beta}{m_{\tilde{t}_2^2} - m_{\tilde{t}_1^2}} \right) \\ &\quad + \frac{3h_b^2}{64\pi^2} |\lambda|^2 s(Q) v_u(Q) (4f_b - 4m_b^2 B'_b g_b),\end{aligned}\quad (17)$$

where  $|\mu| \equiv |\mu_{\text{eff}}|/\sqrt{2} = |\lambda|s(Q)/\sqrt{2}$ ,  $m_t$  and  $m_b$  are the masses of  $t$  and  $b$  quarks, respectively, and the squark masses  $m_{\tilde{q}}$  are given in Appendix A. Also in the above equations

$$\begin{aligned}B_t &= \frac{|A_t| - |\mu| \cot \beta \cos(\phi'_\lambda + \phi_{A_t})}{m_{\tilde{t}_2^2} - m_{\tilde{t}_1^2}}, \quad B_b = \frac{|A_b| - |\mu| \tan \beta \cos(\phi'_\lambda + \phi_{A_b})}{m_{\tilde{b}_2^2} - m_{\tilde{b}_1^2}}, \\ B'_t &= \frac{|A_t|^2 + |\mu|^2 \cot^2 \beta - 2|\mu||A_t| \cot \beta \cos(\phi'_\lambda - \phi_{A_t})}{(m_{\tilde{t}_2^2} - m_{\tilde{t}_1^2})^2}, \\ B'_b &= \frac{|A_b|^2 + |\mu|^2 \tan^2 \beta - 2|\mu||A_b| \tan \beta \cos(\phi'_\lambda - \phi_{A_b})}{(m_{\tilde{b}_2^2} - m_{\tilde{b}_1^2})^2},\end{aligned}\quad (18)$$

and the quantities  $L_{\tilde{f}}, L_{\tilde{f}f}, f_f$  and  $g_f$  are given in Appendix B.  $\mathcal{M}_{SP}^2$  also receives the corresponding corrections given as

$$\begin{aligned}\Delta\mathcal{M}_{SP,11}^2 &= -\frac{3h_b^2 m_b^2}{4\pi^2} \frac{|A_b||\mu| \tan \beta \sin(\phi'_\lambda + \phi_{A_b})}{m_{\tilde{b}_2^2} - m_{\tilde{b}_1^2}} L_{\tilde{b}}, \\ \Delta\mathcal{M}_{SP,22}^2 &= -\frac{3h_t^2 m_t^2}{4\pi^2} \frac{|A_t||\mu| \cot \beta \sin(\phi'_\lambda + \phi_{A_t})}{m_{\tilde{t}_2^2} - m_{\tilde{t}_1^2}} L_{\tilde{t}}, \\ \Delta\mathcal{M}_{SP,12}^2 &= \frac{3h_t^2 m_t^2}{8\pi^2} |\mu| \left( |A_t| B'_t g_t \sin(\phi'_\lambda + \phi_{A_t}) - \frac{|A_t| \sin(\phi'_\lambda + \phi_{A_t})}{m_{\tilde{t}_2^2} - m_{\tilde{t}_1^2}} \right) \\ &\quad + \frac{3h_b^2 m_b^2}{8\pi^2} |\mu| \left( |A_b| B'_b g_b \sin(\phi'_\lambda + \phi_{A_b}) - \frac{|A_b| \sin(\phi'_\lambda + \phi_{A_b})}{m_{\tilde{b}_2^2} - m_{\tilde{b}_1^2}} \right), \\ \Delta\mathcal{M}_{SP,13}^2 &= \frac{3h_b^2 m_b^2 |\lambda| v_u(Q)}{8\sqrt{2}\pi^2} \left( |A_b| B'_b g_b \sin(\phi'_\lambda + \phi_{A_b}) - \frac{|A_b| \sin(\phi'_\lambda + \phi_{A_b})}{m_{\tilde{b}_2^2} - m_{\tilde{b}_1^2}} \right), \\ \Delta\mathcal{M}_{SP,23}^2 &= \frac{3h_t^2 m_t^2 |\lambda| v_d(Q)}{8\sqrt{2}\pi^2} \left( |A_t| B'_t g_t \sin(\phi'_\lambda + \phi_{A_t}) - \frac{|A_t| \sin(\phi'_\lambda + \phi_{A_t})}{m_{\tilde{t}_2^2} - m_{\tilde{t}_1^2}} \right).\end{aligned}\quad (19)$$

There are additional  $D$ -term contributions which are quite involved but do not give large logarithms since the squarks are assumed to have masses close to the ultraviolet cutoff  $M_{\text{SUSY}}^2$ . These corrections are given for  $\mathcal{M}_S^2$  as

$$\begin{aligned}\Delta\mathcal{M}_{S,11}^2 &= 2|\mu| \left( |A_t| C_t \cot \beta \cos(\phi'_\lambda + \phi_{A_t}) - |A_b| C_b \tan \beta \cos(\phi'_\lambda + \phi_{A_b}) \right) \\ &\quad + 2|A_b|^2 C_b + 2D_b - 2|\mu|^2 C_t \cot^2 \beta, \\ \Delta\mathcal{M}_{S,22}^2 &= 2|\mu| \left( |A_b| C_b \tan \beta \cos(\phi'_\lambda + \phi_{A_b}) - |A_t| C_t \cot \beta \cos(\phi'_\lambda + \phi_{A_t}) \right) \\ &\quad + 2|A_t|^2 C_t + 2D_t - 2|\mu|^2 C_b \tan^2 \beta, \\ \Delta\mathcal{M}_{S,12}^2 &= \cot \beta \left( (|\mu|^2 - |A_t|^2) C_t - D_t \right) + \tan \beta \left( (|\mu|^2 - |A_b|^2) C_b - D_b \right) \\ &\quad - |\mu| \left( |A_t| C_t (1 - \cot^2 \beta) \cos(\phi'_\lambda + \phi_{A_t}) + |A_b| C_b (1 - \tan^2 \beta) \cos(\phi'_\lambda + \phi_{A_b}) \right),\end{aligned}$$



$$\begin{aligned}
\Delta\mathcal{M}_{S,13}^2 &= \frac{|\lambda|}{\sqrt{2}} \left( |A_t| C_t v_d(Q) \cot \beta \cos(\phi'_\lambda + \phi_{A_t}) - |A_b| C_b v_u(Q) \cos(\phi'_\lambda + \phi_{A_b}) \right) \\
&\quad + \frac{|\lambda|^2}{2} s(Q) \left( v_u(Q) C_b \tan \beta - v_d(Q) C_t \cot \beta \right), \\
\Delta\mathcal{M}_{S,23}^2 &= \frac{|\lambda|}{\sqrt{2}} \left( |A_b| C_b v_u(Q) \tan \beta \cos(\phi'_\lambda + \phi_{A_b}) - |A_t| C_t v_d(Q) \cos(\phi'_\lambda + \phi_{A_t}) \right) \\
&\quad + \frac{|\lambda|^2}{2} s(Q) \left( v_d(Q) C_t \cot \beta - v_u(Q) C_b \tan \beta \right),
\end{aligned} \tag{20}$$

where again the quantities  $C_f$  and  $D_f$  are defined in Appendix B, and for  $\mathcal{M}_{SP}^2$  as

$$\begin{aligned}
\Delta\mathcal{M}_{SP,11}^2 &= 2|\mu| \left( |A_t| C_t \cot \beta \sin(\phi'_\lambda + \phi_{A_t}) - |A_b| C_b \tan \beta \sin(\phi'_\lambda + \phi_{A_b}) \right), \\
\Delta\mathcal{M}_{SP,22}^2 &= 2|\mu| \left( |A_b| C_b \tan \beta \sin(\phi'_\lambda + \phi_{A_b}) - |A_t| C_t \cot \beta \sin(\phi'_\lambda + \phi_{A_t}) \right), \\
\Delta\mathcal{M}_{SP,12}^2 &= -|\mu| \left( |A_t| C_t (1 - \cot^2 \beta) \sin(\phi'_\lambda + \phi_{A_t}) + |A_b| C_b (1 - \tan^2 \beta) \sin(\phi'_\lambda + \phi_{A_b}) \right), \\
\Delta\mathcal{M}_{SP,13}^2 &= \frac{|\lambda|}{\sqrt{2}} \left( |A_t| C_t v_d \cot \beta \sin(\phi'_\lambda + \phi_{A_t}) - |A_b| C_b v_u \sin(\phi'_\lambda + \phi_{A_b}) \right), \\
\Delta\mathcal{M}_{SP,23}^2 &= \frac{|\lambda|}{\sqrt{2}} \left( |A_b| C_b v_u \tan \beta \sin(\phi'_\lambda + \phi_{A_b}) - |A_t| C_t v_d \sin(\phi'_\lambda + \phi_{A_t}) \right).
\end{aligned} \tag{21}$$

Finally, neglecting all terms without two powers of large logarithms, the dominant two-loop squark contributions to the effective potential can be obtained by integrating the relevant RG equations. These contributions are given as

$$\begin{aligned}
\Delta\mathcal{M}_{S,11}^2 &= \frac{3h_b^4 v_d^2(Q)}{256\pi^4} \left( \ln^2 \left( \frac{M_{\text{SUSY}}^2}{m_t^2} \right) (16g_3^2 - \frac{2}{3}g_1^2 + 3\sin^2 \beta h_t^2 - 3\cos^2 \beta h_b^2) \right. \\
&\quad \left. + \left[ \ln^2 \left( \frac{M_A^2}{m_t^2} \right) - \ln^2 \left( \frac{M_{\text{SUSY}}^2}{m_t^2} \right) \right] (3\sin^2 \beta h_b^2 + (3\sin^2 \beta + 1) h_t^2) \right), \\
\Delta\mathcal{M}_{S,22}^2 &= \frac{3h_t^4 v_u^2(Q)}{256\pi^4} \left( \ln^2 \left( \frac{M_{\text{SUSY}}^2}{m_t^2} \right) (16g_3^2 + \frac{4}{3}g_1^2 - 3\sin^2 \beta h_t^2 + 3\cos^2 \beta h_b^2) \right. \\
&\quad \left. + \left[ \ln^2 \left( \frac{M_A^2}{m_t^2} \right) - \ln^2 \left( \frac{M_{\text{SUSY}}^2}{m_t^2} \right) \right] (3\cos^2 \beta h_t^2 + (3\cos^2 \beta + 1) h_b^2) \right).
\end{aligned} \tag{22}$$

### 2.2.2 Chargino/neutralino, gauge boson and dominant stau contributions

Again, some of the radiative corrections due to the chargino/neutralino loops can be described by an additional shift in  $A_\lambda$  on top of the corrections in Eq. (16),

$$A'_\lambda \rightarrow A''_\lambda = A'_\lambda + \frac{1}{16\pi^2} (g_1^2 M_1 + 3g_2^2 M_2) L_{M_2\mu}, \tag{23}$$

where  $M_1$  and  $M_2$  are the soft gaugino masses, which are taken here to be real. The logarithm  $L_{M_2\mu}$  is defined, along with  $L_{\mu\nu}$ ,  $L_\mu$  and  $L_\nu$  used in the following, in Appendix B. For the CP-odd block in the Higgs mass matrix, all the radiative corrections due to chargino/neutralino loops,  $\sim g^4$ ,



are included by the above shift. The remaining contributions to  $\mathcal{M}_S^2$  are given as

$$\begin{aligned}
\Delta\mathcal{M}_{S,11}^2 &= \frac{1}{16\pi^2} \left[ 2g^2 m_Z^2 \cos^2 \beta (-10 + 16 \sin^2 \theta_W - 8 \sin^4 \theta_W) L_{M_2\mu} \right. \\
&\quad \left. - 4 \left( |\mu|^2 \mathcal{R} \tan \beta + \frac{\lambda^4 m_Z^2 \cos^2 \beta}{g^2} \right) L_{\mu\nu} \right], \\
\Delta\mathcal{M}_{S,22}^2 &= \frac{1}{16\pi^2} \left[ 2g^2 m_Z^2 \sin^2 \beta (-10 + 16 \sin^2 \theta_W - 8 \sin^4 \theta_W) L_{M_2\mu} \right. \\
&\quad \left. - 4 \left( |\mu|^2 \mathcal{R} \cot \beta + \frac{\lambda^4 m_Z^2 \sin^2 \beta}{g^2} \right) L_{\mu\nu} \right], \\
\Delta\mathcal{M}_{S,33}^2 &= \frac{1}{16\pi^2} \left( -32 |\kappa|^2 \nu^2 L_\nu - 8 |\lambda|^2 |\mu|^2 L_\mu \right), \\
\Delta\mathcal{M}_{S,12}^2 &= \frac{1}{16\pi^2} \left[ 4 \left( |\mu|^2 \mathcal{R} - \frac{\lambda^4 m_Z^2 \sin \beta \cos \beta}{g^2} \right) L_{\mu\nu} \right. \\
&\quad \left. - 4g^2 m_Z^2 \sin \beta \cos \beta L_{M_2\mu} \right], \\
\Delta\mathcal{M}_{S,13}^2 &= \frac{1}{16\pi^2} \frac{m_Z s(Q)}{\sqrt{g_1^2 + g_2^2}} \left[ 2 |\lambda|^2 g^2 \cos \beta (-6 + 4 \sin^2 \theta_W) L_{M_2\mu} \right. \\
&\quad \left. + 2\sqrt{2} |\lambda|^2 \left( 2\mathcal{R} \sin \beta - (|\lambda|^2 + 4|\kappa|^2) \cos \beta \right) L_{\mu\nu} \right], \\
\Delta\mathcal{M}_{S,23}^2 &= \frac{1}{16\pi^2} \frac{m_Z s(Q)}{\sqrt{g_1^2 + g_2^2}} \left[ 2 |\lambda|^2 g^2 \sin \beta (-6 + 4 \sin^2 \theta_W) L_{M_2\mu} \right. \\
&\quad \left. + 2\sqrt{2} |\lambda|^2 \left( 2\mathcal{R} \cos \beta - (|\lambda|^2 + 4|\kappa|^2) \sin \beta \right) L_{\mu\nu} \right], \tag{24}
\end{aligned}$$

where  $|\nu| \equiv |\kappa| s(Q)/\sqrt{2}$  and  $m_Z$  is the mass of the  $Z$  boson. The corresponding corrections to  $\mathcal{M}_{SP}^2$  are given as

$$\begin{aligned}
\Delta\mathcal{M}_{S,11}^2 &= -\frac{1}{4\pi^2} |\mu|^2 \mathcal{I} \tan \beta L_{\mu\nu}, \\
\Delta\mathcal{M}_{S,22}^2 &= -\frac{1}{4\pi^2} |\mu|^2 \mathcal{I} \cot \beta L_{\mu\nu}, \\
\Delta\mathcal{M}_{S,12}^2 &= \frac{1}{4\pi^2} |\mu|^2 \mathcal{I} L_{\mu\nu}, \\
\Delta\mathcal{M}_{S,13}^2 &= \frac{1}{2\sqrt{2}\pi^2} \frac{m_Z s(Q)}{\sqrt{g_1^2 + g_2^2}} |\lambda|^2 \mathcal{I} \sin \beta L_{\mu\nu}, \\
\Delta\mathcal{M}_{P,23}^2 &= \frac{1}{2\sqrt{2}\pi^2} \frac{m_Z s(Q)}{\sqrt{g_1^2 + g_2^2}} |\lambda|^2 \mathcal{I} \cos \beta L_{\mu\nu}. \tag{25}
\end{aligned}$$

The contributions from gauge bosons can be conveniently written as

$$\begin{aligned}
\Delta\mathcal{M}_{S,11}^2 &= \Delta_{\text{Gauge}} \cos^2 \beta, \\
\Delta\mathcal{M}_{S,22}^2 &= \Delta_{\text{Gauge}} \sin^2 \beta, \\
\Delta\mathcal{M}_{S,12}^2 &= \Delta_{\text{Gauge}} \sin \beta \cos \beta, \tag{26}
\end{aligned}$$

in terms of the auxiliary quantity

$$\Delta_{\text{Gauge}} = \frac{1}{16\pi^2} g^2 m_Z^2 (-9 + 12 \sin^2 \theta_W - 6 \sin^4 \theta_W) \ln \left( \frac{M_{\text{SUSY}}^2}{m_Z^2} \right). \tag{27}$$

Finally, staus can be considerably lighter than the third generation squarks and hence can give comparatively larger  $D$ -term contributions which are written as

$$\begin{aligned}\Delta\mathcal{M}_{S,11}^2 &= \Delta_{\tilde{\tau}} \cos^2 \beta, \\ \Delta\mathcal{M}_{S,22}^2 &= \Delta_{\tilde{\tau}} \sin^2 \beta, \\ \Delta\mathcal{M}_{S,12}^2 &= -\Delta_{\tilde{\tau}} \sin \beta \cos \beta,\end{aligned}\tag{28}$$

where, assuming a common stau mass,  $m_{\tilde{\tau}}$ ,

$$\Delta_{\tilde{\tau}} = -\frac{1}{16\pi^2} g^2 m_Z^2 (9 \sin^4 \theta_W + 3 \cos^4 \theta_W) \ln \left( \frac{M_{\text{SUSY}}^2}{m_{\tilde{\tau}}^2} \right),\tag{29}$$

with  $\theta_W$  being the weak mixing angle.

### 2.2.3 Wave function renormalisation

As mentioned earlier, the elements of the loop-corrected Higgs mass matrix obtained so far contain VeVs  $v_u(Q)$ ,  $v_d(Q)$  and  $s(Q)$  defined at the scale  $Q^2 = M_{\text{SUSY}}^2$ . These VeVs are related to the VeVs of the properly normalised Higgs fields (i.e., after the addition of quantum effects with  $Q^2 < M_{\text{SUSY}}^2$ ) as

$$v_u(Q) = \frac{v_u}{\sqrt{Z_{H_u}}}, \quad v_d(Q) = \frac{v_d}{\sqrt{Z_{H_d}}}, \quad s(Q) = \frac{s}{\sqrt{Z_S}},\tag{30}$$

where  $Z_i$ , with  $i = H_u, H_d, S$ , are the wave function renormalisation constants. These constants multiply the kinetic terms in the effective action and their explicit forms are given in Appendix B. The elements of the Higgs mass matrix, therefore, have to be rescaled by appropriate powers of these renormalization constants as

$$\mathcal{M}_{H,ij}'^2 = \mathcal{M}_{H,ij}^2 / \sqrt{Z_i Z_j}.\tag{31}$$

This rescaling then takes care of further contributions of the order  $g^2 h_{t,b}^2$  to the Higgs mass matrix.

## 2.3 Physical Higgs boson masses

To obtain the physical mass eigenstates the  $6 \times 6$  Higgs mass matrix  $\mathcal{M}_H'^2$  can be diagonalised using the orthogonal matrix  $O$  as

$$(H_1, H_2, H_3, H_4, H_5, H_6)_a^T = O_{ai} (H_{dR}, H_{uR}, S_R, H_{dI}, H_{uI}, S_I)_i^T.\tag{32}$$

However, one of the resulting states corresponds to a massless Nambu-Goldstone (NG) mode,  $G$ . In order to isolate this NG mode, a  $\beta$  rotation of  $\mathcal{M}_P^2$  is carried out, before the above diagonalisation, as

$$\begin{pmatrix} H_{dI} \\ H_{uI} \\ S_I \end{pmatrix} = \begin{pmatrix} \cos \beta & \sin \beta & 0 \\ -\sin \beta & \cos \beta & 0 \\ 0 & 0 & 1 \end{pmatrix} \begin{pmatrix} G \\ H_I \\ S_I \end{pmatrix}.\tag{33}$$

In the new basis,  $\mathbf{h}^T \equiv (H_{dR}, H_{uR}, S_R, H_I, S_I)$ , after dropping the NG mode, the tree level pseudoscalar block in Eq. (10) gets replaced by

$$\mathcal{M}_{P_\beta}^2 = \begin{pmatrix} (R_\lambda + \mathcal{R}s/2) \frac{v^2 s}{v_d v_u} & (R_\lambda - \mathcal{R}s)v \\ (R_\lambda - \mathcal{R}s)v & R_\lambda \frac{v_d v_u}{s} + 2\mathcal{R}v_d v_u - 3R_\kappa s \end{pmatrix},\tag{34}$$

where  $v = \sqrt{v_u^2 + v_d^2}$ , and the off-diagonal CP-mixing block gets replaced by

$$\mathcal{M}_{SP_\beta}^2 = \begin{pmatrix} 0 & -\frac{3}{2}\mathcal{I}sv_u \\ 0 & -\frac{3}{2}\mathcal{I}sv_d \\ \frac{1}{2}\mathcal{I}sv & -2\mathcal{I}v_uv_d \end{pmatrix}. \quad (35)$$

The radiatively corrected Higgs mass matrix in the new basis can be obtained by similarly  $\beta$ -rotating the mass matrix given in Eq. (31) as

$$\mathcal{M}'_h{}^2 = (\mathcal{M}'_H{}^2)_\beta. \quad (36)$$

The effective potential masses of the neutral Higgs bosons are then obtained by diagonalising the above  $5 \times 5$  mass matrix as  $O'^T \mathcal{M}'_h{}^2 O' = \text{diag}(m_{h_1}^2, m_{h_2}^2, m_{h_3}^2, m_{h_4}^2, m_{h_5}^2)$ , such that

$$m_{h_1}^2 \leq m_{h_2}^2 \leq m_{h_3}^2 \leq m_{h_4}^2 \leq m_{h_5}^2. \quad (37)$$

For Higgs boson pole masses the approximate expression obtained in [20] can be extrapolated to the cNMSSM as

$$\begin{aligned} m_{h_i}^{\text{pole } 2} &= m_{h_i}^2 - \frac{3h_t^2}{16\pi^2} \left[ (m_{h_i}^2 - 4m_t^2) O_{i2}^2 + m_{h_i}^2 O_{i5}^2 \right] B(m_{h_i}^2, m_t^2) \\ &- \frac{3h_b^2}{16\pi^2} \left[ m_{h_i}^2 (O_{i1}^2 + O_{i4}^2) \ln \left( \frac{m_t^2}{m_b^2} \right) + ((m_{h_i}^2 - 4m_b^2) O_{i1}^2 + m_{h_i}^2 O_{i4}^2) B(m_{h_i}^2, m_b^2) \right], \end{aligned} \quad (38)$$

where the function  $B(M^2, m^2)$  is defined as

$$B(M^2, m^2) = \begin{cases} 2 - \sqrt{1 - \frac{4m^2}{M^2}} \ln \left( \frac{1 + \sqrt{1 - \frac{4m^2}{M^2}}}{1 - \sqrt{1 - \frac{4m^2}{M^2}}} \right) : & M^2 > 4m^2, \\ 2 - 2\sqrt{\frac{4m^2}{M^2} - 1} \arctan \left( \sqrt{\frac{M^2}{4m^2 - M^2}} \right) : & M^2 < 4m^2. \end{cases} \quad (39)$$

In the case of the charged Higgs states, a  $\beta$  rotation is also carried out for isolating the NG modes. The corrections to the charged Higgs boson mass, of the order  $h_{t,b}^4$  and those induced by chargino/neutralino, gauge boson and slepton loops give rise to some additional terms on top of the shifts of  $A_\lambda$  described earlier. After including these corrections and  $\beta$ -rotating, the mass of the physical charged Higgs boson is given as

$$\begin{aligned} \mathcal{M}'_\pm{}^2 &= \left[ (R_\lambda + \mathcal{R}s/2)s + v_u(Q)v_d(Q) \left( \frac{g_2^2}{2} - |\lambda|^2 \right) \right] \left( \frac{v_u(Q)}{Z_{H_d}v_d(Q)} + \frac{v_d(Q)}{Z_{H_u}v_u(Q)} \right) \\ &+ \frac{v_u^2(Q) + v_d^2(Q)}{16\pi^2} \left[ 6h_t^2 h_b^2 \ln \left( \frac{M_{\text{SUSY}}^2}{m_t^2} \right) - \frac{3}{4}g_2^4 \ln \left( \frac{M_{\text{SUSY}}^2}{m_l^2} \right) \right. \\ &\left. + \frac{7g_1^2 g_2^2 - g_2^4}{4} \ln \left( \frac{M_{\text{SUSY}}^2}{m_Z^2} \right) + 2(g_1^2 g_2^2 - g_2^4) L_{M_{2\mu}} \right], \end{aligned} \quad (40)$$

where the rescaling by the wave function normalisation constants has been taken care of. The pole mass of the charged Higgs boson is then obtained as

$$\begin{aligned} m_{h^\pm}^{\text{pole } 2} &= \mathcal{M}'_\pm{}^2 + \frac{3}{16\pi^2} \left\{ (h_t^2 \cos^2 \beta + h_b^2 \sin^2 \beta) \left( \mathcal{M}'_\pm{}^2 \left[ \left( 1 - \frac{m_t^2}{\mathcal{M}'_\pm{}^2} \right) \ln \left| \frac{\mathcal{M}'_\pm{}^2 - m_t^2}{m_t^2} \right| - 2 \right] \right. \right. \\ &+ (m_t^2 + m_b^2) \left[ \left( 1 - \frac{m_t^2}{\mathcal{M}'_\pm{}^2} \right) \ln \left| \frac{m_t^2}{\mathcal{M}'_\pm{}^2 - m_t^2} \right| + 1 \right] \Bigg) \\ &\left. + \frac{4m_t^2 m_b^2}{v^2} \left[ \left( 1 - \frac{m_t^2}{\mathcal{M}'_\pm{}^2} \right) \ln \left| \frac{m_t^2}{\mathcal{M}'_\pm{}^2 - m_t^2} \right| + 1 \right] \right\}. \end{aligned} \quad (41)$$

### 3 Trilinear Higgs boson self-interactions

The complete NMSSM Lagrangian contains the interaction terms of the Higgs bosons with the fermions, scalars and vector bosons as well as with each other, from which the corresponding couplings can be obtained. In table 1 we summarize various Higgs boson couplings which will be used in the expressions for neutral Higgs boson decay widths in the next section. The analytical formulae for these couplings in the cNMSSM, with the exception of the Higgs boson self-couplings, can be found in [32]. The couplings between three neutral Higgs bosons, obtained from the potential in Eq. (3), are given as

$$\begin{aligned}
g_{h_a h_b h_c} = & \frac{g^2}{4} \left( v_u (\Pi_{abc}^{111} - \Pi_{abc}^{122} + \Pi_{abc}^{144} - \Pi_{abc}^{155}) + v_d (\Pi_{abc}^{222} - \Pi_{abc}^{211} + \Pi_{abc}^{255} - \Pi_{abc}^{244}) \right) \\
& + \frac{\lambda^2}{2} \left( v_u (\Pi_{abc}^{122} + \Pi_{abc}^{133} + \Pi_{abc}^{155} + \Pi_{abc}^{166}) + v_d (\Pi_{abc}^{211} + \Pi_{abc}^{233} + \Pi_{abc}^{244} + \Pi_{abc}^{266}) \right. \\
& \left. + s (\Pi_{abc}^{311} + \Pi_{abc}^{322} + \Pi_{abc}^{344} + \Pi_{abc}^{355}) \right) + \kappa^2 s \left( \Pi_{abc}^{333} + \Pi_{abc}^{366} \right) \\
& - R_\lambda \left( \Pi_{abc}^{123} - \Pi_{abc}^{453} - \Pi_{abc}^{426} - \Pi_{abc}^{156} \right) + R_\kappa \left( \Pi_{abc}^{333} - 3\Pi_{abc}^{366} \right) \\
& - \frac{\mathcal{R}}{2} \left( v_u (\Pi_{abc}^{233} - \Pi_{abc}^{266} + 2\Pi_{abc}^{536}) + v_d (\Pi_{abc}^{133} - \Pi_{abc}^{166} + \Pi_{abc}^{436}) \right. \\
& \left. + 2s (\Pi_{abc}^{123} - \Pi_{abc}^{345} + \Pi_{abc}^{156} + \Pi_{abc}^{426}) \right) \\
& - \frac{\mathcal{I}}{2} \left( v_u (\Pi_{abc}^{566} - \Pi_{abc}^{533} + 2\Pi_{abc}^{236}) + v_d (\Pi_{abc}^{466} - \Pi_{abc}^{433} + \Pi_{abc}^{136}) \right. \\
& \left. + s (3\Pi_{abc}^{126} - 3\Pi_{abc}^{456} - \Pi_{abc}^{135} - \Pi_{abc}^{423}) + 3\frac{v_d v_u}{s} (\Pi_{abc}^{666} - \Pi_{abc}^{336}) \right), \tag{42}
\end{aligned}$$

where

$$\Pi_{abc}^{ijk} = O_{ai} O_{bj} O_{ck} + O_{ai} O_{cj} O_{bk} + O_{bi} O_{aj} O_{ck} + O_{bi} O_{cj} O_{ak} + O_{ci} O_{aj} O_{bk} + O_{ci} O_{bj} O_{ak}, \tag{43}$$

with  $O_{xy}$  being the elements of the Higgs mixing matrix defined in Eq. (32). The couplings of the neutral Higgs bosons to a pair of charged Higgs bosons are similarly given as

$$\begin{aligned}
g_{h_a h^+ h^-} = & \frac{g_1^2}{8} \left( v_u (\Pi_{abc}^{111} - \Pi_{abc}^{122}) + v_d (\Pi_{abc}^{222} - \Pi_{abc}^{211}) \right) \\
& + \frac{g_2^2}{8} \left( v_u (\Pi_{abc}^{111} + \Pi_{abc}^{122} + 2\Pi_{abc}^{212}) + v_d (\Pi_{abc}^{222} + \Pi_{abc}^{211} + 2\Pi_{abc}^{112}) \right) \\
& + \frac{\lambda^2}{2} \left( s (\Pi_{abc}^{311} + \Pi_{abc}^{322}) - v_u \Pi_{abc}^{212} - v_d \Pi_{abc}^{112} \right) \\
& + \mathcal{R} s \Pi_{abc}^{312} + R_\lambda \Pi_{abc}^{312} + \frac{3}{2} \mathcal{I} s \Pi_{abc}^{612}, \tag{44}
\end{aligned}$$

where

$$\Pi_{abc}^{ijk} = 2O_{ai} C_j C_k \text{ with } C_1 = \cos \beta, C_2 = \sin \beta. \tag{45}$$

### 4 Neutral Higgs boson decays

In this section, we present the analytical expressions for the decay widths of the cNMSSM Higgs bosons into pairs of fermions, massive gauge bosons, sfermions, photons, gluons and lighter Higgs

<i>fermion pair</i>	$g_{h_a \bar{f} f}^S$	$g_{h_a \bar{f} f}^P$
$d\bar{d}/l^+l^-$	$O_{a1}/\cos\beta$	$-O_{a4}/\cos\beta$
$u\bar{u}$	$O_{a2}/\sin\beta$	$-O_{a5}/\sin\beta$
$\tilde{\chi}_j^0 \tilde{\chi}_k^0$	$g_{h_a \tilde{\chi}_j^0 \tilde{\chi}_k^0}^S$	$g_{h_a \tilde{\chi}_j^0 \tilde{\chi}_k^0}^P$
$\tilde{\chi}_j^- \tilde{\chi}_k^+$	$g_{h_a \tilde{\chi}_j^- \tilde{\chi}_k^+}^S$	$g_{h_a \tilde{\chi}_j^- \tilde{\chi}_k^+}^P$
<i>sfermions</i>	$g_{h_a \tilde{f}_b \tilde{f}_c^*}$	
<i>gauge bosons</i>	$g_{h_a VV}$	
<i>Higgs + Z boson</i>	$g_{h_a h_b Z}$	
<i>neutral Higgs bosons</i>	$g_{h_a h_b h_c}$	
<i>charged Higgs bosons</i>	$g_{h_a h^+ h^-}$	

Table 1: The couplings of the NMSSM Higgs boson  $h_a$  to particles and sparticles at the tree level.  $g_{h_a \bar{f} f}^S$  and  $g_{h_a \bar{f} f}^P$  refer to vector and axial vector couplings of the fermions, respectively.  $O_{ai}$  are the elements of the Higgs mixing matrix defined in Sect. 2.3.

bosons as well as into a lighter Higgs and massive gauge boson pair. These expressions have mostly been adopted from [34] and follow the notation therein. For the decay modes involving an off-mass-shell gauge boson, three-body decays are described following [35].

•  $h \rightarrow ff'$

The decay width of a Higgs boson into two fermions is given as

$$\begin{aligned}
\Gamma(h_a \rightarrow ff') &= N_C \frac{G_F M_{h_a} \lambda^{1/2}(1, \kappa_{af}, \kappa_{af'})}{4\sqrt{2}\pi} \bar{m}_q^2(m_{h_a}) \Gamma_M K_a^f \\
&\times [(1 - \kappa_{af} - \kappa_{af'}) (|g_{h_a ff'}^S|^2 + |g_{h_a ff'}^P|^2) \\
&- 2\sqrt{\kappa_{af} \kappa_{af'}} (|g_{h_a ff'}^S|^2 - |g_{h_a ff'}^P|^2)] ,
\end{aligned} \tag{46}$$

where  $G_F/\sqrt{2} = g_2^2/8m_W^2$ , with  $m_W$  being the  $W$  boson mass,  $\kappa_{af^{(\prime)}}$   $\equiv m_{f^{(\prime)}}^2/m_{h_a}^2$ ,  $\lambda(1, x, y) \equiv (1 - x - y)^2 - 4xy$  and the couplings  $g_{h_a ff'}^S$  and  $g_{h_a ff'}^P$  have been defined in table 1 (where  $f' = \bar{f}$  in the case of quarks and leptons). The colour factor  $N_C$  is equal to 3 for quarks and to 1 for leptons, charginos and neutralinos.  $\Gamma_M = \left(\frac{4}{1+\delta_{bc}}\right)$  for Majorana fermions such as (s)neutrinos, neutralinos and charginos, with  $\delta_{bc} = 1$  when they are identical, while for Dirac fermions  $\Gamma_M = 1$ . For  $h_a \rightarrow q\bar{q}$  the leading-order QCD corrections are taken into account with the enhancement factor  $K_a^q = 1 + 5.67 \frac{\alpha_s(m_{h_a}^2)}{\pi}$ . For leptons, neutralinos and charginos,  $K_a^f = 1$ .

•  $h \rightarrow VV$

The decay width into two massive gauge bosons is given as

$$\Gamma(h_a \rightarrow VV) = \delta_V \frac{G_F g_{h_a VV}^2 m_{h_a}^3}{16\sqrt{2}\pi} \beta_{iV} (1 - 4\kappa_{aV} + 12\kappa_{aV}^2), \tag{47}$$

where  $\kappa_{aV} = m_V^2/m_{h_a}^2$ ,  $\beta_{aV} = \sqrt{1 - 4\kappa_{aV}}$ ,  $\delta_W = 2$  and  $\delta_Z = m_W^4/(\cos\theta_W m_Z)^4 = 1$ . Below the  $VV$  threshold, when one of the gauge bosons is off mass shell, the three-body decay width of a

Higgs boson is given as

$$\Gamma(h_a \rightarrow VV^*) = \delta'_V \frac{3G_F g_{h_a VV}^2 m_{h_a} m_V^4}{16\sqrt{2}\pi} R(\kappa_a V), \quad (48)$$

where  $\delta'_W = 2$ ,  $\delta'_Z = 7/12 - 10 \sin^2 \theta_W / 9 + 40 \sin^4 \theta_W / 27$  and

$$R(x) = 3 \frac{1 - 8x + 20x^2}{\sqrt{4x - 1}} \arccos \left( \frac{3x - 1}{2x^{3/2}} \right) - \frac{1 - x}{2x} (2 - 13x + 47x^2) - \frac{3}{2} (1 - 6x + 4x^2) \log x. \quad (49)$$

•  $h_a \rightarrow h_b h_c, \tilde{f}_b \tilde{f}_c^*$

The decay width of a Higgs boson into two scalar particles, including sfermions and lighter Higgs bosons, is written as

$$\Gamma(h_a \rightarrow h_b h_c, \tilde{f}_b \tilde{f}_c^*) = \frac{N_F |\mathcal{G}|^2}{16\pi m_{h_a}} \lambda^{1/2} (1, \kappa_{ab}, \kappa_{ac}), \quad (50)$$

where  $(N_F, \mathcal{G}) = (1/(1 + \delta_{bc}), g_{h_a h_b h_c})$ ,  $(N_C, g_{h_a \tilde{f}_b \tilde{f}_c^*})$  and  $\kappa_{ai} = m_{h_i, \tilde{f}_i}^2 / m_{h_a}^2$ .

•  $h_a \rightarrow h_b Z$

The decay width of a Higgs boson into a lighter Higgs and  $Z$  boson pair is given as

$$\Gamma(h_a \rightarrow h_b Z) = g_{h_a h_b Z}^2 \frac{G_F m_Z^4}{8\sqrt{2}\pi m_{h_a}} \sqrt{\lambda'(m_{h_b}^2, m_Z^2; m_{h_a}^2)} \lambda'(m_{h_b}^2, m_{h_a}^2; m_Z^2), \quad (51)$$

where the function  $\lambda'(x, y; z) = (1 - x/z - y/z)^2 - 4xy/z^2$ . Below the threshold for the above process, the three-body decay width is given as

$$\Gamma(h_a \rightarrow h_b Z^*) = g_{h_a h_b Z}^2 \delta'_Z \frac{9G_F^2 m_Z^4 m_{h_a}}{16\pi^3} G_{h_b Z}, \quad (52)$$

where the generic functions  $G_{ij}$  can be written as

$$G_{ij} = \frac{1}{4} \left\{ 2(-1 + \kappa_j - \kappa_i) \sqrt{\lambda_{ij}} \left[ \frac{\pi}{2} + \arctan \left( \frac{\kappa_j(1 - \kappa_j + \kappa_i) - \lambda_{ij}}{(1 - \kappa_i) \sqrt{\lambda_{ij}}} \right) \right] \right. \\ \left. + (\lambda_{ij} - 2\kappa_i) \log \kappa_i + \frac{1}{3}(1 - \kappa_i) \left[ 5(1 + \kappa_i) - 4\kappa_j + \frac{2}{\kappa_j} \lambda_{ij} \right] \right\}, \quad (53)$$

using the parameters

$$\lambda_{ij} = -1 + 2\kappa_i + 2\kappa_j - (\kappa_i - \kappa_j)^2; \quad \kappa_i = \frac{m_i^2}{m_{h_a}^2}. \quad (54)$$

•  $h \rightarrow Z\gamma$

The decay width of a Higgs boson into a  $Z$  boson and photon pair is given by

$$\Gamma(h_a \rightarrow Z\gamma) = \frac{G_F m_W^2 \alpha^2 m_{h_a}^3}{64\pi^3} (1 - \kappa_{aZ})^3 \left[ |S_a^{Z\gamma}(m_{h_a})|^2 + |P_a^{Z\gamma}(m_{h_a})|^2 \right]. \quad (55)$$

In the above expression the scalar and pseudoscalar form factors, retaining only the dominant loop contributions, which include those from  $t$  and  $b$  quarks,  $W^\pm$  and  $H^\pm$ , are given by

$$\begin{aligned} S_a^{Z\gamma}(m_{h_a}) &= \sum_{f=b,t} g_{h_a \bar{f} f}^S F'_{sf}(\tau_{af}, \lambda_f) + g_{h_a VV} F'_1(\tau_{aW}, \lambda_W) \\ &\quad + \frac{g_{h_a h^+ h^-}}{2\sqrt{2}G_F m_{h^\pm}^2} F'_0(\tau_{ah^\pm}, \lambda_{h^\pm}), \\ P_a^{Z\gamma}(m_{h_a}) &= \sum_{f=b,t} g_{h_a \bar{f} f}^P F'_{pf}(\tau_{af}, \lambda_f), \end{aligned} \quad (56)$$

where  $\tau_{ax} = 4m_x^2/m_{h_a}^2$  and  $\lambda_x = 4m_x^2/m_Z^2$ . The form factors  $F'_{sf}$ ,  $F'_{pf}$ ,  $F'_0$  and  $F'_1$  are given as

$$\begin{aligned} F'_{sf}(\tau, \lambda) &= 6 \frac{Q_f(I_{3f} - 2Q_f \sin^2 \theta_W)}{\cos \theta_W} [I_1(\tau, \lambda) - I_2(\tau, \lambda)], \\ F'_{pf}(\tau, \lambda) &= 12 \frac{Q_f(I_{3f} - 2Q_f \sin^2 \theta_W)}{\cos \theta_W} I_2(\tau, \lambda), \\ F'_0(\tau, \lambda) &= \frac{\cos 2\theta_W}{\cos \theta_W} I_1(\tau, \lambda), \\ F'_1(\tau, \lambda) &= \cos \theta_W \left\{ 4(3 - \tan^2 \theta_W) I_2(\tau, \lambda) \right. \\ &\quad \left. + \left[ \left(1 + \frac{2}{\tau}\right) \tan^2 \theta_W - \left(5 + \frac{2}{\tau}\right) \right] I_1(\tau, \lambda) \right\}, \end{aligned} \quad (57)$$

where  $Q_f$  is the electric charge of the fermion  $f$  and  $I_{3f}$  is the third component of its isospin. The functions  $I_{1,2}$  are defined as

$$I_1(\tau, \lambda) = \frac{\tau\lambda}{2(\tau - \lambda)} + \frac{\tau^2\lambda^2}{2(\tau - \lambda)^2} [f(\tau) - f(\lambda)] + \frac{\tau^2\lambda}{(\tau - \lambda)^2} [g(\tau) - g(\lambda)], \quad (58)$$

$$I_2(\tau, \lambda) = -\frac{\tau\lambda}{2(\tau - \lambda)} [f(\tau) - f(\lambda)], \quad (59)$$

with

$$g(\tau) = \begin{cases} \sqrt{\tau - 1} \arcsin \frac{1}{\sqrt{\tau}} & \tau \geq 1 \\ \frac{\sqrt{1 - \tau}}{2} \left[ \log \frac{1 + \sqrt{1 - \tau}}{1 - \sqrt{1 - \tau}} - i\pi \right] & \tau < 1. \end{cases} \quad (60)$$

#### • $h \rightarrow \gamma\gamma$

The decay width into two photons is given as

$$\Gamma(h_a \rightarrow \gamma\gamma) = \frac{G_F \alpha^2 m_{h_a}^3}{128\sqrt{2}\pi^3} \left[ |S_a^\gamma(m_{h_a})|^2 + |P_a^\gamma(m_{h_a})|^2 \right], \quad (61)$$



where  $\alpha$  is the fine-structure constant. The scalar and pseudoscalar form factors, retaining only the loop contributions from  $W^\pm$ ,  $H^\pm$  and the dominant ones from (s)fermions, are given by

$$\begin{aligned}
S_a^\gamma(m_{h_a}) &= 2 \sum_{f=b,t,\tilde{\chi}_1^\pm,\tilde{\chi}_2^\pm} N_C Q_f^2 g_{h_a\bar{f}f}^S F_{sf}(\tau_{af}) \\
&+ \sum_{\tilde{f}_j=\tilde{t}_1,\tilde{t}_2,\tilde{b}_1,\tilde{b}_2,\tilde{\tau}_1,\tilde{\tau}_2} N_C Q_f^2 \frac{g_{H_i\tilde{f}_j^*\tilde{f}_j}}{2\sqrt{2}G_F m_{\tilde{f}_j}^2} F_0(\tau_{a\tilde{f}_j}) \\
&+ g_{h_a VV} F_1(\tau_{aW}) + \frac{g_{h_a h^+ h^-}}{2\sqrt{2}G_F m_{h^\pm}^2} F_0(\tau_{ah^\pm}), \\
P_a^\gamma(m_{h_a}) &= 2 \sum_{f=b,t,\tilde{\chi}_1^\pm,\tilde{\chi}_2^\pm} N_C Q_f^2 g_{h_a\bar{f}f}^P F_{pf}(\tau_{af}).
\end{aligned} \tag{62}$$

The form factors  $F_{sf}$ ,  $F_{pf}$ ,  $F_0$  and  $F_1$  in the above equations are given as

$$\begin{aligned}
F_{sf}(\tau) &= \tau [1 + (1 - \tau)f(\tau)], \quad F_{pf}(\tau) = \tau f(\tau), \\
F_0(\tau) &= -\tau [1 - \tau f(\tau)], \quad F_1(\tau) = -[2 + 3\tau + 3\tau(2 - \tau)f(\tau)],
\end{aligned} \tag{63}$$

in terms of the scaling function  $f(\tau)$  written as

$$f(\tau) = \begin{cases} \arcsin^2\left(\frac{1}{\sqrt{\tau}}\right) : & \tau \geq 1, \\ -\frac{1}{4} \left[ \ln\left(\frac{1+\sqrt{1-\tau}}{1-\sqrt{1-\tau}}\right) - i\pi \right]^2 : & \tau < 1. \end{cases} \tag{64}$$

•  $h \rightarrow gg$

The decay width of a Higgs boson into two gluons is given by

$$\Gamma(h_a \rightarrow gg) = \frac{G_F \alpha_S^2 m_{h_a}^3}{16\sqrt{2}\pi^3} \left[ K_S^g |S_a^g(m_{h_a})|^2 + K_P^g |P_a^g(m_{h_a})|^2 \right], \tag{65}$$

where  $\alpha_S$  is the strong coupling constant and the scalar and pseudoscalar form factors, retaining only the contributions from third generation (s)quarks, are given by

$$\begin{aligned}
S_a^g(m_{h_a}) &= \sum_{f=b,t} g_{h_a f\bar{f}}^S F_{sf}(\tau_{af}) + \sum_{\tilde{f}_j=\tilde{t}_1,\tilde{t}_2,\tilde{b}_1,\tilde{b}_2} \frac{g_{h_a\tilde{f}_j^*\tilde{f}_j}}{4\sqrt{2}G_F m_{\tilde{f}_j}^2} F_0(\tau_{a\tilde{f}_j}), \\
P_a^g(m_{h_a}) &= \sum_{f=b,t} g_{h_a f\bar{f}}^P F_{pf}(\tau_{af}),
\end{aligned} \tag{66}$$

with functions  $F_{sf}$ ,  $F_{pf}$  and  $F_0$ , being the same as for the  $\gamma\gamma$  mode above.  $K_{S,P}^g$  in Eq. (65) are QCD loop enhancement factors that include the leading-order QCD corrections. In the heavy-quark limit, the factors  $K_{H,A}^g$  are given by [36]

$$\begin{aligned}
K_S^g &= 1 + \frac{\alpha_S(M_{H_i}^2)}{\pi} \left( \frac{95}{4} - \frac{7}{6} N_F \right), \\
K_P^g &= 1 + \frac{\alpha_S(M_{H_i}^2)}{\pi} \left( \frac{97}{4} - \frac{7}{6} N_F \right),
\end{aligned} \tag{67}$$

where  $N_F$  is the number of quark flavours lighter than the  $h_a$  boson.

## 5 Novel heavy Higgs boson decays into SM-like 125 GeV states

In this section we discuss a cNMSSM scenario which, if probed at the LHC, could provide an indication of not only the existence of CP violation in the Higgs sector but also of a non-minimal nature of SUSY. For a numerical analysis of this scenario, we use a fortran program (available on request) in which the Higgs mass matrix calculated above has been implemented along with other SUSY mass matrices (given in Appendix A). This program computes the particle mass spectrum for a given set of the cNMSSM input parameters defined at  $M_{\text{SUSY}}$ . In addition, all the expressions for decay widths, as given in the previous section, have been implemented in the program, enabling it to also calculate Higgs boson BRs in various decays modes. In the current version of the program, QCD corrections have been included only in the decays into quarks and gluons via  $K$ -factors, as noted in eqs. (46) and (67) respectively. In the CPC limit, the Higgs boson masses and BRs have been compared with those given by NMSSMTools-v3.2.4 [33] (with the flag for precision in the calculation of Higgs boson masses set to the default value of 0). While the mass calculations have been found to differ by  $\sim 1\%$  at the most between the two programs, the differences in BRs can reach as high as  $\sim 5\%$  for some points. This is mainly because of a more robust treatment of QCD corrections in NMSSMTools, which is not straightforwardly extendable to the CPV case.

We also note here that the extension of further corrections to the Higgs boson masses, those from Higgs loop contributions and those calculated in [37] for the real NMSSM (included in NMSSMTools by setting the Higgs boson mass precision flag to 2), to the cNMSSM in the effective potential approach is a work in progress. However, while such improved precision may slightly alter the regions of the model parameter space yielding the correct mass of the signal candidate Higgs boson, the results obtained here for our scenario of interest, which is a generic feature of the cNMSSM, should still largely be valid in those regions.

Our package also tests the output of a given point in the cNMSSM parameter space against the constraints from the direct searches of the SM (and SUSY) Higgs boson(s) as well as third generation squark, stau and light chargino at the large electron positron (LEP) collider. Although no limits from  $b$ -physics, LHC SUSY searches or from relic density measurements have so far been implemented in the package, in our current analysis we confine ourselves to points from among those which have been found to best comply with such constraints (see, e.g., [22, 23, 38, 39]).

In the experimental searches the magnitude of the signal is typically characterized by the ‘signal strength’,  $\mu(X) \equiv \sigma_{\text{obs}}(X)/\sigma_{h_{\text{SM}}}(X)$ , where  $h_{\text{SM}}$  implies a SM Higgs boson with a mass equal to the measured one of the observed boson decaying via a given channel  $X$ . The theoretical counterpart of this quantity, sometimes referred to as the *reduced cross section*, for a Higgs boson,  $h_i$ , produced in the dominant gluon fusion mode is given as

$$\mu_{h_i}(X) = \frac{\sigma(gg \rightarrow h_i)}{\sigma(gg \rightarrow h_{\text{SM}})} \times \frac{\text{BR}(h_i \rightarrow X)}{\text{BR}(h_{\text{SM}} \rightarrow X)}. \quad (68)$$

To a good approximation, the ratio of the production cross sections  $\sigma$  of  $h_i$  and  $h_{\text{SM}}$  in the above expression can be substituted by the ratio of their respective decay widths into two gluons. We, therefore, redefine the reduced cross section as

$$R_{h_i}(X) \equiv \frac{\Gamma(h_i \rightarrow gg)}{\Gamma(h_{\text{SM}} \rightarrow gg)} \times \frac{\text{BR}(h_i \rightarrow X)}{\text{BR}(h_{\text{SM}} \rightarrow X)}, \quad (69)$$

which is calculated by the program for each of the Higgs bosons of the model. For the Higgs bosons that are assumed to have escaped detection so far,  $R_{h_i}(X)$  is tested against the LHC exclusion limit on  $\mu(X)$  wherever it is available for a given decay channel. In case two Higgs bosons of the model are so close in mass that the event excesses due to each of them cannot be independently

resolved by the experiment,  $R_{h_i}(X)$  is simply taken to be the sum of their individual reduced cross sections.

As noted earlier, the presence of non-zero CPV phases in the Higgs sector of the NMSSM can result in some unique scenarios which are not possible when CP is conserved. In particular, a decrease in the mass of a given Higgs boson with a variation in CPV phases can result in the kinematical opening of new decay channels. Conversely, a gradual decrease in the Higgs boson mass can result in the closing of a particular decay channel beyond a certain value of a given CPV phase, thereby causing a notable reduction in its total width and a deviation in its BRs from the CPC case. Indeed such deviations were observed for a  $\sim 125$  GeV SM-like Higgs boson in [27], owing sometimes to the contribution of the CPV phases to the gaugino masses also besides the Higgs boson mass itself. Another crucial possibility arises due to the fact that the Higgs mass eigenstates do not carry a definite CP assignment for non-zero CPV phases. Hence, couplings between pseudoscalar and scalar states which are forbidden in the CPC limit become possible upon the introduction of such phases, resulting in some ‘unconventional’ Higgs boson decays.

In the NMSSM, in analogy with the decoupling regime of the MSSM, when one of the CP-even Higgs bosons is required to have exactly SM-like couplings and a mass around 125 GeV the other doublet-like scalar and pseudoscalar Higgs bosons are typically very heavy,  $\gtrsim 500$  GeV. In this case a correlation exists between the masses of the light doublet-like and the singlet-like scalar Higgs bosons such that the latter is either lighter than the former, in a small portion of the parameter space, or decoupled like the other heavy doublet-like Higgs bosons. On the other hand, the mass of the singlet-like pseudoscalar, typically  $a_1$ , approximated at the leading order (for large  $\tan\beta$ ) by

$$m_{a_1}^2 \simeq -\kappa s A_\kappa, \quad (70)$$

can vary much more freely depending on the size of the parameter  $A_\kappa$ , with marginal effect on the masses of the other Higgs bosons. It is thus possible for  $a_1$  to have a mass close to twice that of the SM-like Higgs boson. Note also the fact that the partial decay width of a given Higgs boson,  $h_a$ , into two lighter Higgs bosons, given in Eq. (51), is inversely proportional to  $m_{h_a}$ . Hence, when CPV phases are turned on, the decay amplitude of a (now CP-indefinite)  $\sim 250$  GeV Higgs boson into a pair of SM-like Higgs bosons is non-vanishing. Evidently, lower mass of  $a_1$  also implies the availability of more, albeit still rather small, phase space for its production.

In the following we will further discuss the representative points of three benchmark cNMSSM parameter space cases wherein not only a SM-like  $\sim 125$  GeV Higgs boson but also the above mentioned  $\sim 250$  GeV Higgs boson can be obtained. We will analyse in detail the impact of variation in the CPV phase  $\phi'_\kappa$  (we fix  $\varphi$  to  $0^\circ$  so that  $\phi'_\kappa = \phi_\kappa$ )<sup>1</sup> on the properties of the relevant Higgs bosons for these points. We should indicate here that the chosen points exhibiting our scenario of interest are indeed not isolated ones and dedicated scans of their neighbourhoods in the model parameter space should reveal many more similar points. However, such scans are beyond the scope of this article since our aim here is to highlight some specific characteristics of the parameter regions yielding our representative points, rather than to map out their sizes. For convenience, we shall refer to the singlet-like pseudoscalar(-like) Higgs boson generically as  $h_p$ , to the  $\sim 125$  GeV SM-like Higgs boson as  $h_d$  and to the other singlet-dominated scalar(-like) boson as  $h_s$  henceforth.

In principle, since the coupling of  $h_p$  to a pair of  $h_d$  is only induced by CPV phases one can expect the corresponding partial decay width and BR to be minimal. However, as noted above,

---

<sup>1</sup>Since only the difference  $\phi'_\lambda - \phi'_\kappa$  enters the Higgs mass matrix at the tree level, the variation in Higgs boson properties with varying  $\phi'_\kappa$  is almost identical to that with varying  $\phi'_\lambda$ , as was noted in [27]. However, since  $\phi'_\kappa$  is virtually unconstrained by the measurements of fermionic EDMs [32, 30], we only vary this phase in our analysis. Also, since  $\phi_{A_0}$  does not contribute directly to the Higgs-to-Higgs decay width, its relevance to our scenario under consideration is minimal.

the fact that the mass of  $h_p$  lies much closer to the  $h_d h_d$  production threshold than that of the heavy doublet-like Higgs bosons is crucial and provides a unique possibility in the context of Higgs boson phenomenology at the LHC. Therefore, for quantifying the magnitude of the process where  $h_p$  produced via gluon fusion decays into one or more  $h_d$  which subsequently decay in the channel  $X$ , we compute, following Eq. (69), the auxiliary quantity

$$A_i^{h_p}(\gamma\gamma) \equiv \frac{\Gamma(h_p \rightarrow gg)}{\Gamma(h_{\text{SM}} \rightarrow gg)} \times \text{BR}(h_p \rightarrow h_d h_i) \times \frac{\text{BR}(h_d \rightarrow \gamma\gamma)}{\text{BR}(h_{\text{SM}} \rightarrow \gamma\gamma)}, \quad (71)$$

where  $h_{\text{SM}}$  refers to a SM Higgs boson with the same mass as  $h_d$ .  $i = d, s$  in the above equation, since the decay  $h_p \rightarrow h_d h_s$  is also possible when  $m_{h_s} < m_{h_p} - m_{h_d}$ . The second of the two Higgs bosons thus produced, whether  $h_d$  or  $h_s$ , is assumed to have escaped undetected in the recent run of LHC, since no Higgs pair production has been observed there. It can, however, be probed mainly in the  $b\bar{b}$  decay channel, as discussed in [40], in the next LHC run with  $\sqrt{s} = 14$  TeV. We, therefore, also calculate the corresponding auxiliary rate for this Higgs boson in the  $b\bar{b}$  channel. Evidently both  $A_d^{h_p}(\gamma\gamma)$  and  $A_s^{h_p}(\gamma\gamma)$  are by definition zero in the CPC limit. We stress here that the above expression gives only a crude estimate of diphoton production rate via this channel, since the incoming gluons will require a larger momentum fraction for producing the heavier  $h_p$  than for  $h_{\text{SM}}$  and thus their structure functions will differ. However, while a calculation of the actual total cross section for the process  $h_p \rightarrow h_d h_i \rightarrow X_1 X_2$  is needed for an accurate estimate of its significance at the LHC, the above expression provides a reasonably good approximation since  $h_p$  in our scenario of interest is not much heavier than  $h_d$ . Evidently then, such an auxiliary signal rate cannot be defined for the other, much heavier, Higgs bosons of the model.

Furthermore, in our analysis below we will compute  $R_{h_d}(X)$ , defined in Eq. (69), for  $X = \gamma\gamma, ZZ, \tau^+ \tau^-$  for each benchmark case as a measure of the deviation of  $h_d$  from SM-like properties.  $R_{h_d}(X) = 1$  thus implies that  $h_d$  has an exactly SM-like signal strength in the channel  $X$ . As for the SUSY inputs, we will impose the mSUGRA-inspired unification conditions,

$$\begin{aligned} M_0 &\equiv M_{Q_3} = M_{U_3} = M_{D_3} = M_{L_3} = M_{E_3} = M_{\text{SUSY}}, \\ M_{1/2} &\equiv 2M_1 = M_2 = \frac{1}{3}M_3, \\ A_0 &\equiv A_t = A_b = A_\tau, \end{aligned}$$

where  $M_{Q_3}^2, M_{U_3}^2, M_{D_3}^2$  and  $M_{L_3}^2, M_{E_3}^2$  are the soft SUSY-breaking squared masses of the third generation squarks and sleptons, respectively. Finally, we will fix  $\text{sign}[\cos(\phi_\lambda + \phi_{A_\lambda})] = \text{sign}[\cos(\phi_\kappa + \phi_{A_\kappa})] = +1$ .

### 5.1 $h_1 = h_d$

We first discuss the case when the lightest Higgs state,  $h_1$ , is SM-like while  $h_p$  is the second lightest of the five neutral Higgs states of the model, hence corresponding to  $h_2$ . As a representative of this case we choose the point P1, given in table 2, in the cNMSSM parameter space. This point yields  $h_d$  around 125 GeV in the CPC limit, with almost exactly SM-like signal strengths in the  $\gamma\gamma, ZZ$  and  $\tau^+ \tau^-$  channels, despite a non-vanishing  $\lambda$  and, hence, singlet component (such a NMSSM Higgs boson has been discussed in [43]). In panel (a) of figure 1 we show the auxiliary signal rates  $A_d^{h_p}(\gamma\gamma)$  and  $A_d^{h_p}(b\bar{b})$  as functions of  $\phi_\kappa$  for P1. We see that the lines corresponding to these two signal rates overlap each other exactly. Both these rates rise gradually and reach a maximum value,  $\sim 0.07$ , for  $\phi_\kappa = 29^\circ$ . Such a  $h_p$  can thus be responsible for up to 7% of the observed  $\gamma\gamma$  excess besides that due to the direct production of  $h_d$  in the gluon fusion channel. The increase in  $A_d^{h_p}(\gamma\gamma)$

---

<sup>2</sup>A  $\sim 4\sigma$  evidence of a  $\sim 125$  GeV Higgs boson has now also been established in the  $\tau^+ \tau^-$  channel [41, 42].

Point	$M_0$	$M_{1/2}$	$A_0$	$\tan \beta$	$\lambda$	$\kappa$	$\mu_{\text{eff}}$	$A_\lambda$	$A_\kappa$
P1	2500	1300	-6000	12	0.09	0.11	1000	600	-30
P2	2500	1000	-3000	20	0.04	0.013	200	200	-200
P3	1000	500	-2500	2	0.54	0.34	140	185	-200

Table 2: Values of the cNMSSM parameters corresponding to the three benchmark cases discussed in the text. All dimensionful parameters are in units of GeV.

and  $A_d^{h_p}(b\bar{b})$  with  $\phi_\kappa$  is a twofold consequence of the gradual increase in the gluonic width of  $h_p$  and an increase in its BR into the  $h_d$  pair. The reason for the cutoff in the line is that beyond  $\phi_\kappa = 29^\circ$  the minimization condition given in Eq. (9) is not satisfied any more.

In panel (b) we show the signal strength of  $h_p$ , produced via gluon fusion, in the  $\gamma\gamma$ ,  $ZZ$  and  $\tau^+\tau^-$  decay channels. We note that although there is a considerable rise in  $R_{h_p}$ , particularly in the  $\gamma\gamma$  and  $ZZ$  channels, with an increasing amount of CP violation, these rates barely exceed the per mil level for allowed values of  $\phi_\kappa$ . This is due to the fact that  $h_p$  has a significantly reduced coupling to two photons compared to that of a SM Higgs boson with the same mass. In panel (c) there are shown the dominant BRs of  $h_p$  against its mass, with  $\phi_\kappa$  increasing from left to right. This plot demonstrates the main reason of large auxiliary signal rates of  $h_p$  for non-zero  $\phi_\kappa$ , as observed above. We see that as soon as the process  $h_p \rightarrow h_d h_d$  is allowed, it becomes one of the dominant decay modes of  $h_p$ , with BR reaching up to  $\sim 0.23$ . However, it is still not the most dominant decay mode due to the fact that  $h_p$  develops non-zero couplings also to gauge boson pairs. Therefore, the decay  $h_p \rightarrow W^+W^-$  has the highest BR for non-zero  $\phi_\kappa$ , while the BR of  $h_p$  into  $ZZ$  also lies close to that into  $h_d h_d$ . As a result, the decay modes  $h_p \rightarrow b\bar{b}$  and  $h_p \rightarrow \tau^+\tau^-$ , which had the highest and second highest BRs, respectively, in the CPC limit, become very subdominant. Since there is a negligible increase in the mass of  $h_p$  with increasing  $\phi_\kappa$ , all the above BRs remain almost constant over the entire allowed range of this phase.

Finally, in panel (d) we show the signal strengths of  $h_d$  in the  $\gamma\gamma$ ,  $ZZ$  and  $\tau^+\tau^-$  channels plotted against its mass. With increasing  $\phi_\kappa$  (again, from left to right)  $m_{h_d}$  falls slowly. It reaches  $\sim 125$  GeV for  $\phi_\kappa = 29^\circ$ , hence becoming more consistent with the mass measurements at the LHC [44, 45] (which, nevertheless have appreciable experimental errors). We see in the figure that the signal strengths of  $h_d$  in all three decay modes considered are very SM-like in the CPC limit and show a very slow drop with increasing  $\phi_\kappa$ .

## 5.2 $h_2 = h_d$

As stated in the Introduction, in the NMSSM the  $h_2$  (the second lightest scalar in the CPC limit) can also be the  $\sim 125$  GeV SM-like Higgs boson with the  $h_1$  corresponding to  $h_s$ . Below, we discuss two distinct cases, based on the compositions of  $h_1$  and  $h_2$ , in which this possibility is realised.

Small singlet-doublet mixing: For small  $\lambda$ ,  $\kappa$  and  $\mu_{\text{eff}}$  but intermediate-to-large  $\tan \beta$ ,  $h_2$  is still doublet-dominated and hence possesses very SM-like couplings to fermions and bosons. In this case, due to a smaller VeV  $s$  resulting from a lower value of  $\mu_{\text{eff}}$  (recall that  $\mu_{\text{eff}} = \lambda s$ ) compared to the case discussed above, the mass of the singlet-like scalar Higgs boson falls below that of  $h_d$ . In fact, owing to a highly dominant singlet component,  $m_{h_s}$  can reach very low values,  $\sim 40$  GeV, before it violates the LEP limit on  $hZ$  production [46]. This effectively bounds  $m_{h_p}$ , which grows with increasing  $A_\kappa$  while  $m_{h_s}$  falls, from above. Thus it is extremely difficult for  $A_\kappa$  and, resultantly,

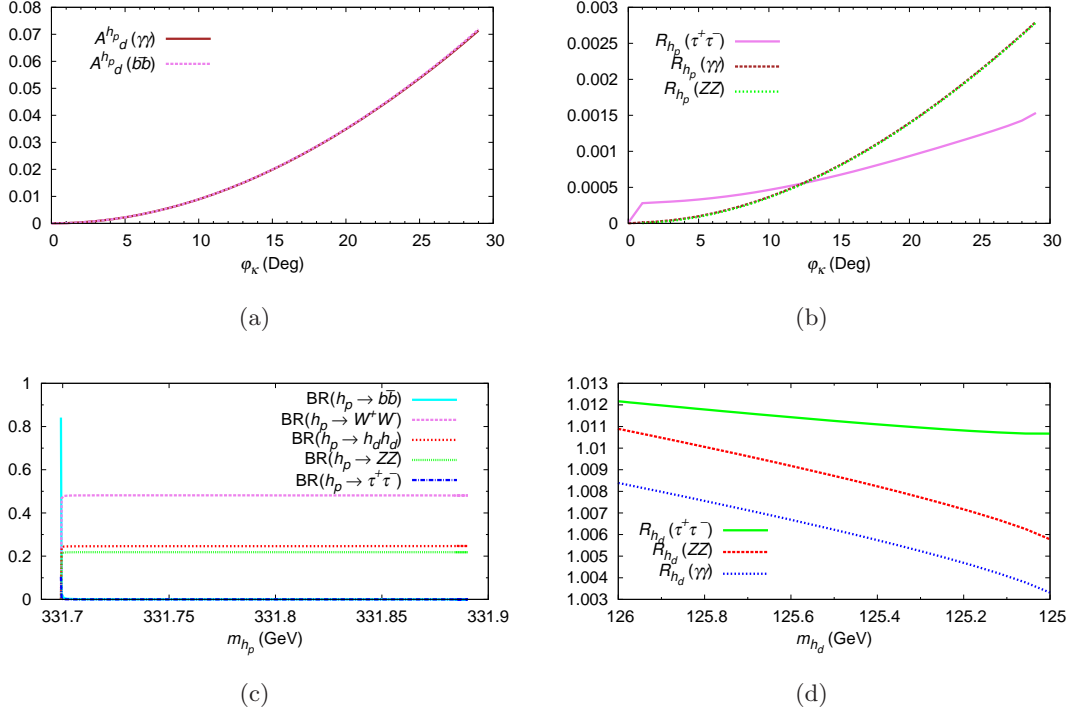


Figure 1: Case when  $h_1 = h_d$  and  $h_2 = h_p$ . (a) Auxiliary rates  $A_d^{h_p}(\gamma\gamma)$  (solid brown line) and  $A_d^{h_p}(b\bar{b})$  (dashed violet line) as functions of  $\phi_\kappa$ , for  $h_d h_d$  pair production. (b)  $R_{h_p}(\tau^+\tau^-)$  (solid violet line),  $R_{h_p}(\gamma\gamma)$  (dashed brown line) and  $R_{h_p}(ZZ)$  (dotted green line) as functions of  $\phi_\kappa$ . (c) BRs of  $h_p$  into  $b\bar{b}$  (solid cyan line),  $W^+W^-$  (dashed violet line),  $h_d h_d$  (large-dotted red line),  $ZZ$  (small-dotted green line) and  $\tau^+\tau^-$  (dot-dashed blue line) vs  $m_{h_p}$ . (d) Signal strengths of  $h_d$  in the  $\tau^+\tau^-$  channel (solid green line), in the  $ZZ$  channel (dashed red line) and in the  $\gamma\gamma$  channel (dotted blue line) vs  $m_{h_d}$ .

$m_{h_p}$  to become large enough to allow the  $h_p \rightarrow h_d h_d$  decay. However, thanks to a fairly light  $h_s$ , the decay  $h_p \rightarrow h_d h_s$  is alternatively possible for non-zero  $\phi_\kappa$ .

We choose the point P2, with its coordinates in the cNMSSM parameter space given in table 2, to demonstrate the effects of CP violation on the phenomenology of  $h_p$  for this case. In panel (a) of figure 2 we show  $A_d^{h_p}(\gamma\gamma)$  against  $\phi_\kappa$  for P2. We see in the figure that  $A_d^{h_p}(\gamma\gamma)$  grows steadily until  $\phi_\kappa = 40^\circ$  after which it falls abruptly. The reason for this fall is the opening up of the  $h_p \rightarrow \chi_1 \chi_1$  decay channel as we shall see below. Note that even the peak value of  $A_d^{h_p}(\gamma\gamma)$  for  $\phi_\kappa = 40^\circ$  in this case lies two orders of magnitude below the per mil level. The line has been artificially cut off at  $\phi_\kappa = 90^\circ$  since the auxiliary rate remains almost steady afterwards. In panel (b)  $A_s^{h_p}(b\bar{b})$  is shown for the second Higgs boson,  $h_s$ , produced along with  $h_d$  against  $\phi_\kappa$ . The auxiliary rate via this Higgs boson is always lower than that of  $h_d$  on account of its being singlet-dominated and hence coupling very weakly to matter. In panel (c) we show the direct production signal rates of  $h_p$  in the  $\gamma\gamma$ ,  $ZZ$  and  $\tau^+\tau^-$  channels against  $\phi_\kappa$ . While  $R_{h_p}(\gamma\gamma)$  and  $R_{h_p}(ZZ)$  remain almost of the same order as the auxiliary rate via  $h_d$ ,  $R_{h_p}(\tau^+\tau^-)$  rises much more briskly with increasing  $\phi_\kappa$  and reaches the per mil level for  $\phi_\kappa \sim 40^\circ$ .

The reason for the sudden drop in the various signal rates of  $h_p$  after  $\phi_\kappa = 40^\circ$  becomes obvious from panel (d), where we show its dominant BRs plotted against  $m_{h_p}$ . In contrast with the first



case above, even when the  $h_p \rightarrow h_d h_s$  decay channel opens up for non-zero  $\phi_\kappa$ , it remains very subdominant, with BR still smaller than that for the  $h_p \rightarrow b\bar{b}$  mode. We see in the figure that for small non-zero values of  $\phi_\kappa$  the decay mode  $h_p \rightarrow W^+ W^-$  is clearly the most dominant one, with BR as high as  $\sim 0.7$ , while  $h_p \rightarrow ZZ$  is the second most dominant mode. With increasing  $\phi_\kappa$  (left to right)  $m_{h_p}$  falls negligibly, but just before it reaches 187.86 GeV, the  $\text{BR}(h_p \rightarrow \chi_1 \chi_1)$  suddenly shoots up. This is a consequence of the fact that  $m_{\chi_1}$  also falls sharply as  $\phi_\kappa$  is increased, so much so that for  $\phi_\kappa > 40^\circ$   $\chi_1$  becomes light enough to make the decay of  $h_p$  into its pair possible kinematically. Resultantly, beyond  $\phi_\kappa = 40^\circ$  all the hitherto dominant decay modes,  $h_p \rightarrow W^+ W^-$ ,  $h_p \rightarrow ZZ$  and  $h_p \rightarrow b\bar{b}$ , become more and more subdominant while the  $\text{BR}(h_p \rightarrow h_d h_s)$  falls even further.

The above discussion of the behaviour of various BRs of  $h_p$  has an important implication, that  $\chi_1$ , at least for large values of  $\phi_\kappa$ , is highly singlino-dominated. It should, therefore, be extremely difficult to be probed at a direct detection experiment for dark matter, such as XENON [47]. In panel (e) we show the signal strengths of  $h_d$  against its mass for this case. The mass  $m_{h_d}$  increases slowly with increasing  $\phi_\kappa$ , conversely to P1, while  $R_{h_d}(ZZ)$  and  $R_{h_d}(\gamma\gamma)$  fall gradually. These two rates never drop below 0.9 and hence always lie well within the experimental uncertainties around the measured central values at the LHC.  $R_{h_d}(\tau^+ \tau^-)$ , on the other hand, is always much higher than  $R_{h_d}(ZZ)$  and  $R_{h_d}(\gamma\gamma)$  and closer to 1 for all values of  $\phi_\kappa$ . Finally, in panel (f) there are shown the signal strengths of the accompanying  $h_s$  in the same three decay channels. Conversely to the  $h_d$  rates,  $R_{h_s}(\tau^+ \tau^-)$  is much lower than  $R_{h_s}(ZZ)$  and  $R_{h_s}(\gamma\gamma)$ , with all these rates lying just above the percent level for  $\phi_\kappa = 0^\circ$ . The rates rise slowly with increasing  $\phi_\kappa$  until it reaches  $40^\circ$ , after which they become almost steady.

Large singlet-doublet mixing: It was noted in [22] that, for large  $\lambda$  and  $\kappa$  and small  $\tan \beta$  and  $\mu_{\text{eff}}$ ,  $h_2$  in the NMSSM (again,  $h_d$  here) can have a considerably enhanced  $\gamma\gamma$  rate compared to  $h_{\text{SM}}$ , due mainly to the reduced coupling and consequently reduced  $\text{BR}(h_d \rightarrow b\bar{b})$ . This scenario, in which the  $h_1$  ( $h_s$  here) has a mass lying just below  $m_{h_2}$  [23] and the lightest stop can have a mass significantly below 1 TeV [39], is sometimes referred to as the ‘natural NMSSM’ [48]. To discuss the impact of a light  $h_p$  on such a scenario in the cNMSSM we choose the point P3, given in table 2.

Unlike in the second case discussed above, in this case  $h_p$  can easily have a mass more than twice that of  $h_d$ , implying that its decay into  $h_d h_d$  is possible simultaneously with that into  $h_d h_s$ , once CP is violated. In panel (a) of figure 3 we show  $A_d^{h_p}(\gamma\gamma)$  and  $A_d^{h_p}(b\bar{b})$  when a pair of  $h_d$  is produced via  $h_p$  decay, as functions of the phase  $\phi_\kappa$ . We see that  $A_d^{h_p}(\gamma\gamma)$  grows rapidly with increasing  $\phi_\kappa$ , reaching  $\sim 0.07$  for  $\phi_\kappa = 5^\circ$ .  $A_d^{h_p}(b\bar{b})$  also grows, although relatively slowly, with increasing  $\phi_\kappa$ , which is cut off at  $5^\circ$  due to the fact that  $m_{h_d}$  falls sharply, as we shall see later, and for larger values of the phase it becomes incompatible with the current LHC measurements of the Higgs boson mass. At the same time, the mass of  $h_s$ , which has a significant doublet component due to the large  $\lambda$ , also violates the LEP bound mentioned earlier. In panel (b) we show  $A_d^{h_p}(\gamma\gamma)$  and  $A_s^{h_p}(b\bar{b})$  when, alternatively, a  $h_d h_s$  pair is produced via  $h_p$  decay, as functions of  $\phi_\kappa$ . In this case the two auxiliary rates rise to much larger values for  $\phi_\kappa = 5^\circ$  compared to the case of  $h_d h_d$  pair production seen in panel (a). Notably, while  $A_d^{h_p}(\gamma\gamma)$  reaches a peak value of 0.25,  $A_s^{h_p}(b\bar{b})$  also rises to about 0.12, owing to the fact that  $h_s$  here has a considerably larger doublet component compared to the above case with small singlet-doublet mixing. Panel (c) shows that  $R_{h_p}(\gamma\gamma)$  for this case also rises to percent level for  $\phi_\kappa > 1^\circ$  and reaches a peak value of  $\sim 0.07$ .  $R_{h_p}(ZZ)$  and  $R_{h_p}(\tau^+ \tau^-)$  also rise slowly, with the latter barely exceeding the per mil level for  $\phi_\kappa = 5^\circ$ .

In panel (d) of figure 3 we show the  $\text{BR}(h_p \rightarrow h_d h_d)$  and the  $\text{BR}(h_p \rightarrow h_d h_s)$  plotted against  $m_{h_p}$ , with  $\phi_\kappa$  increasing from left to right. In contrast with the earlier cases, we see that neither of



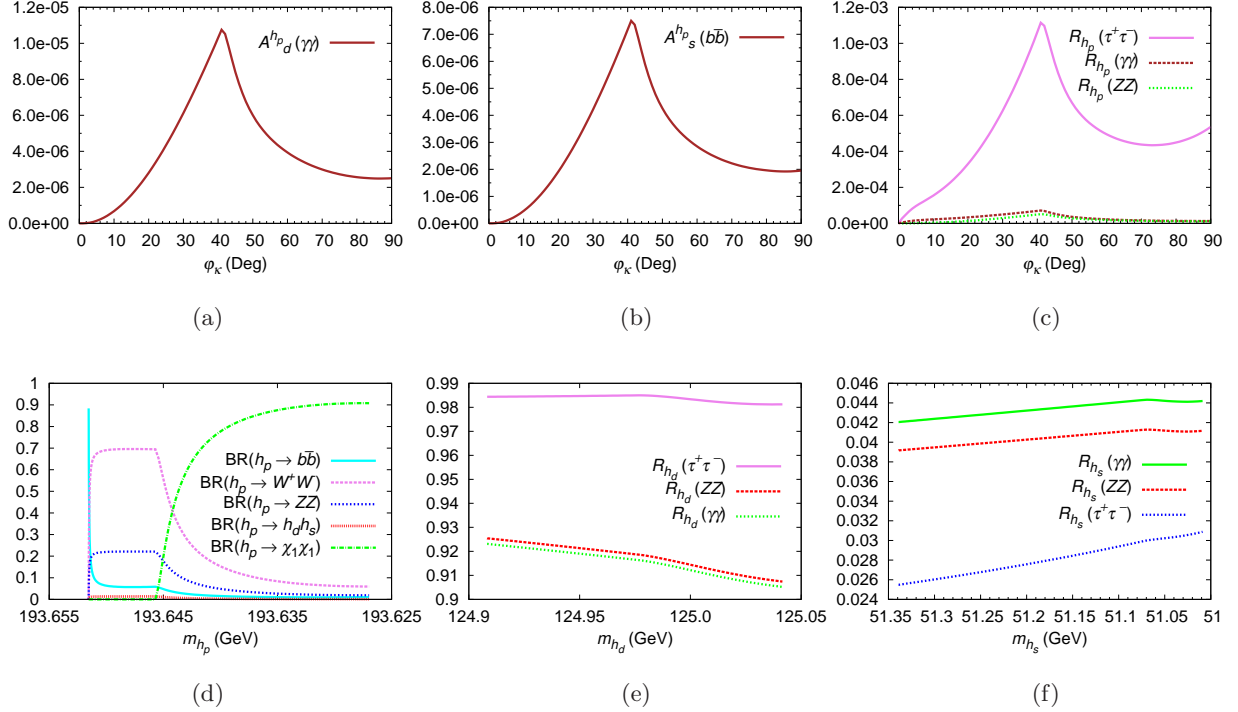


Figure 2: Case when  $h_2 = h_d$  with small singlet-doublet mixing and  $h_3 = h_p$ . (a), (b) Auxiliary rates  $A_d^{h_p}(\gamma\gamma)$  and  $A_s^{h_p}(b\bar{b})$ , respectively, as functions of  $\phi_\kappa$ , for  $h_d h_s$  pair production. (c)  $R_{h_p}(\tau^+\tau^-)$  (solid violet line),  $R_{h_p}(\gamma\gamma)$  (dashed brown line) and  $R_{h_p}(ZZ)$  (dotted green line) as functions of  $\phi_\kappa$ . (d) BRs of  $h_p$  into  $b\bar{b}$  (solid cyan line),  $W^+W^-$  (dashed violet line),  $ZZ$  (large-dotted blue line),  $h_d h_s$  (small-dotted red line) and  $\chi_1\chi_1$  (dot-dashed green line) vs  $m_{h_p}$ . (e) Signal strengths of  $h_d$  in the  $\tau^+\tau^-$  channel (solid violet line), in the  $ZZ$  channel (dashed red line) and in the  $\gamma\gamma$  channel (dotted green line) vs  $m_{h_d}$ . (f) Signal strengths of  $h_s$  in the  $\gamma\gamma$  channel (solid green line), in the  $ZZ$  channel (dashed red line) and in the  $\tau^+\tau^-$  channel (dotted blue line) vs  $m_{h_s}$ .

these two BRs reaches a value even as high as 0.04, even though they still yield significant  $A^{h_p}(\gamma\gamma)$  rates as noted above. The  $\text{BR}(h_p \rightarrow h_d h_d)$  is dominant over the  $\text{BR}(h_p \rightarrow h_d h_s)$  for  $\phi_\kappa \leq 4^\circ$ , but becomes subdominant for larger  $\phi_\kappa$ , owing to the fact that  $m_{h_s}$  starts falling faster than  $m_{h_d}$ . The reason for small BRs of  $h_p$  in these two decay modes becomes clear, once again, when one looks at the other BRs, shown in panel (e) against  $m_{h_s}$ . We see in the figure that the  $\text{BR}(h_p \rightarrow \chi_1\chi_1)$  is always highly dominant. In fact for  $\phi_\kappa = 0^\circ$   $h_p$  almost always decays into a pair of  $\chi_1$ . With increasing  $\phi_\kappa$   $m_{h_s}$  starts falling and, consequently, the  $\text{BR}(h_p \rightarrow h_s h_s)$  starts rising. At the same time the  $\text{BR}(h_p \rightarrow W^+W^-)$  and the  $\text{BR}(h_p \rightarrow ZZ)$  also rise slowly, while the  $\text{BR}(h_p \rightarrow \chi_1\chi_1)$  drops sharply, although it still remains the most dominant one for almost the entire allowed range of  $\phi_\kappa$ . Only for  $\phi_\kappa = 5^\circ$  the BR of hitherto the third dominant decay mode,  $h_p \rightarrow W^+W^-$ , rises slightly above the BRs of both  $h_p \rightarrow \chi_1\chi_1$  and  $h_p \rightarrow h_s h_s$  and becomes the most dominant one,  $\sim 0.3$ .

Finally, in panel (f) we show the signal strengths for both  $h_d$  and  $h_s$  in the  $\gamma\gamma$ ,  $ZZ$  and  $\tau^+\tau^-$  channels against their respective masses for this case. We see that  $m_{h_d}$  falls quite sharply with increasing  $\phi_\kappa$ , again in contrast with the earlier cases, which is one of the reasons for  $\phi_\kappa$  being restricted to values of  $\mathcal{O}(1)$ , as noted earlier. Additionally,  $R_{h_d}(ZZ)$  is not only smaller than  $R_{h_d}(\gamma\gamma)$

when CP is conserved but it also behaves quite differently with increasing  $\phi_\kappa$ .  $R_{h_d}(\gamma\gamma)$ , already significantly above 1 in the CPC limit, slowly increases further with increasing  $\phi_\kappa$  while  $R_{h_d}(ZZ)$ , also slightly above 1 initially, grows more SM-like by falling slowly. Expectedly,  $R_{h_d}(\tau^+\tau^-)$  is already below 1 in the CPC limit owing to the large singlet component of  $h_d$  and, consequently, a reduced coupling to fermions. It falls further with increasing  $\phi_\kappa$  and deviates considerably from a SM-like rate for the maximum allowed value of the phase. As for  $h_s$ , its mass also drops with increasing  $\phi_\kappa$  but its signal rates in the three decay channels considered rise continuously. In fact,  $R_{h_s}(\tau^+\tau^-)$  reaches as high as  $\sim 0.5$  for  $\phi_\kappa = 5^\circ$  while  $R_{h_s}(\gamma\gamma)$  and  $R_{h_s}(ZZ)$  also reach up to 0.2.

One may thus deduce in this case that non-zero values of  $\phi_\kappa$  are already tightly constrained by the LHC Higgs boson data. This is due to the dual fact that such values push  $R_{h_d}(\gamma\gamma)$ , which is already on the larger side in the CPC limit, upward, and  $R_{h_d}(\tau^+\tau^-)$ , which is already on the smaller side in the CPC limit, further downward. However, it should be noted that any further enhancement in the  $\gamma\gamma$  rate is only slight with increasing  $\phi_\kappa$ , particularly for  $\phi_\kappa < 4^\circ$ , so that it is still consistent with the ATLAS measurement,  $\mu(\gamma\gamma) = 1.6 \pm 0.3$  [45]. The same can be said for the signal strengths of  $h_d$  and  $h_s$  in the  $\tau^+\tau^-$  channel. For smaller non-zero values of  $\phi_\kappa$   $R_{h_d}(\tau^+\tau^-)$  ( $R_{h_s}(\tau^+\tau^-)$ ) is still large (small) enough to be consistent with (excluded by) the LHC data, taking into account the experimental errors on the measurements. Nevertheless, of the three cases discussed here, while this case presents the possibility of the largest contribution by  $h_p$  to  $h_d$  production at the LHC, it is the weakest in that the signal strengths of the Higgs bosons predicted by it lie at the verge of being excluded.

## 6 Summary and outlook

In this article we have presented the one-loop Higgs mass matrix of the complex NMSSM in the RG-improved effective potential approach, along with the expressions for Higgs boson trilinear self-couplings. We have then highlighted a scenario, precluded in the MSSM, wherein the decay of a pseudoscalar-like Higgs boson into 125 GeV Higgs bosons is induced by non-zero values of the CPV phase  $\phi_\kappa$ . We have noted that, when one of the scalar Higgs bosons is required to have a SM-like signal rate, it is relatively easy for the mass of the singlet-pseudoscalar-like Higgs boson to be near  $\sim 250$  GeV compared to the other heavy Higgs bosons of the model. The fact that the decay width of a heavy Higgs boson into two lighter ones is inversely proportional to its mass renders such a  $\sim 250$  GeV Higgs boson particularly interesting as well as relevant for the phenomenology of the SM-like Higgs boson in the model.

We have analysed three benchmark cases corresponding to different parameter configurations in the NMSSM which generate a  $\sim 125$  GeV SM-like Higgs boson and a pseudoscalar near 250 GeV. In our analysis the impact of non-zero CPV phases in each of these cases is quantified in terms of an auxiliary signal rate  $A^{h_p}(\gamma\gamma)$ . This approximate quantity assumes that the  $\sim 250$  GeV pseudoscalar-like Higgs boson is produced in the gluon fusion mode at the LHC and decays into a (pair of) SM-like Higgs boson(s), one of which subsequently decays into a photon pair. By calculating this auxiliary rate in each case studied, we have deduced that such a  $\sim 250$  GeV Higgs boson can generally contribute significantly to the production of SM-like Higgs bosons at the LHC for large CPV phases. In fact, in one of the cases discussed, the auxiliary signal rate for this Higgs boson can be as high as 25% of the observed  $\gamma\gamma$  rate.

Evidently, a calculation of the total cross section for our considered process is essential to draw concrete inferences about its observability or significance at the LHC. In this regard, a calculation of higher order corrections to the Higgs trilinear couplings in the complex NMSSM, following those derived in [49] for the real NMSSM, could prove crucial. Furthermore, a detailed study of the signal

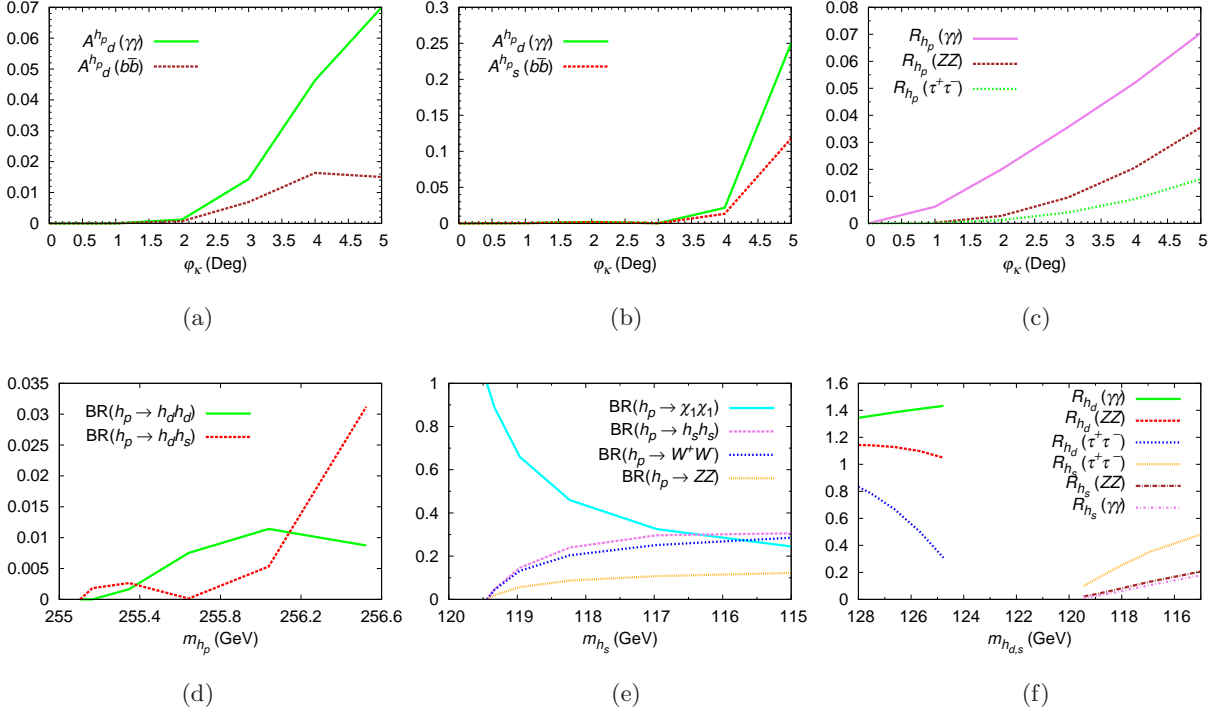


Figure 3: Case when  $h_2 = h_d$  with large singlet-doublet mixing and  $h_3 = h_p$ . (a) Auxiliary rates  $A_d^{h_p}(\gamma\gamma)$  (solid green line) and  $A_d^{h_p}(b\bar{b})$  (dashed brown line) as functions of  $\phi_\kappa$ , for  $h_d h_d$  pair production. (b)  $A_d^{h_p}(\gamma\gamma)$  (solid green line) and  $A_s^{h_p}(b\bar{b})$  (dashed red line) as functions of  $\phi_\kappa$ , for  $h_d h_s$  pair production. (c) Signal strengths  $R_{h_p}(\gamma\gamma)$  (solid violet line),  $R_{h_p}(ZZ)$  (dashed brown line) and  $R_{h_p}(\tau^+\tau^-)$  (dotted green line) as functions of  $\phi_\kappa$ . (d) BRs of  $h_p$  into  $h_d h_d$  (solid green line) and  $h_d h_s$  (dashed red line) vs  $m_{h_p}$ . (e) BRs of  $h_p$  into  $\chi_1 \chi_1$  (solid cyan line),  $h_s h_s$  (dashed violet line),  $W^+ W^-$  (large-dotted blue line) and  $ZZ$  (small-dotted orange line) vs  $m_{h_s}$ . (f)  $R_{h_d}(\gamma\gamma)$  (solid green line),  $R_{h_d}(ZZ)$  (dashed red line),  $R_{h_d}(\tau^+\tau^-)$  (large-dotted blue line),  $R_{h_s}(\tau^+\tau^-)$  (small-dotted orange line),  $R_{h_s}(ZZ)$  (dot-large-dashed brown line) and  $R_{h_s}(\gamma\gamma)$  (dot-small-dashed violet line) vs  $m_{h_{d,s}}$ .

topologies in various channels due to the production of multiple Higgs bosons, in line with the ones studied recently in [48, 40, 50], is also in order. For this purpose, we eventually aim to embed the cNMSSM in a publicly available tool such as CalcHEP [51] to make possible the calculation of actual cross sections in this model. Our current analysis, nevertheless, serves as a clear and timely demonstration of the fact that CP violation in the Higgs sector can be a very important probe of new physics at the LHC. Of particular relevance here is the observation that the  $\sim 250$  GeV Higgs boson mostly has a very poor signal strength when decaying itself into a photon pair but a large BR into lighter Higgs bosons for non-zero CPV phases. Thus, the already observed SM-like Higgs boson could provide an important, and possibly the only, handle on such a beyond-the-SM (and MSSM) scenario.

## Acknowledgements

The author is thankful to S. Moretti for his valuable comments and suggestions for the improvement of this draft. SM is funded in part by the Welcome Programme of the Foundation for Polish Science.

## A Sparticle mass matrices

- The chargino mass matrix, in the  $(\tilde{W}^-, \tilde{H}^-)$  basis, using the convention  $\tilde{H}_{L(R)}^- = \tilde{H}_{d(u)}^-$ , can be written as

$$\mathcal{M}_C = \begin{pmatrix} M_2 & \sqrt{2}M_W \cos \beta \\ \sqrt{2}M_W \sin \beta & \frac{|\lambda|v_S}{\sqrt{2}} e^{i\phi'_\lambda} \end{pmatrix}, \quad (\text{A.1})$$

which is diagonalised by two different unitary matrices as  $C_R \mathcal{M}_C C_L^\dagger = \text{diag}\{m_{\tilde{\chi}_1^\pm}, m_{\tilde{\chi}_2^\pm}\}$ , where  $m_{\tilde{\chi}_1^\pm} \leq m_{\tilde{\chi}_2^\pm}$ .

- The neutralino mass matrix, in the  $(\tilde{B}, \tilde{W}^0, \tilde{H}_d^0, \tilde{H}_u^0, \tilde{S})$  basis, can be written as

$$\mathcal{M}_N = \begin{pmatrix} M_1 & 0 & -m_Z \cos \beta s_W & m_Z \sin \beta s_W & 0 \\ 0 & M_2 & m_Z \cos \beta c_W & -m_Z \sin \beta c_W & 0 \\ -m_Z \cos \beta s_W & m_Z \cos \beta c_W & 0 & -\frac{|\lambda|v_S}{\sqrt{2}} e^{i\phi'_\lambda} & -\frac{|\lambda|v_{S\beta}}{\sqrt{2}} e^{i\phi'_\lambda} \\ m_Z \sin \beta s_W & -m_Z \sin \beta c_W & -\frac{|\lambda|v_S}{\sqrt{2}} e^{i\phi'_\lambda} & 0 & -\frac{|\lambda|v \cos \beta}{\sqrt{2}} e^{i\phi'_\lambda} \\ 0 & 0 & -\frac{|\lambda|v_{S\beta}}{\sqrt{2}} e^{i\phi'_\lambda} & -\frac{|\lambda|v \cos \beta}{\sqrt{2}} e^{i\phi'_\lambda} & \sqrt{2}|\kappa|v_S e^{i\phi'_\kappa} \end{pmatrix}, \quad (\text{A.2})$$

where  $s_W = \sin \theta_W$ , with  $\theta_W$  being the Weinberg angle. The above matrix is diagonalised as  $N^* \mathcal{M}_N N^\dagger = \text{diag}(m_{\tilde{\chi}_1^0}, m_{\tilde{\chi}_2^0}, m_{\tilde{\chi}_3^0}, m_{\tilde{\chi}_4^0}, m_{\tilde{\chi}_5^0})$ , where  $N$  is a unitary matrix and  $m_{\tilde{\chi}_1^0} \leq m_{\tilde{\chi}_2^0} \leq m_{\tilde{\chi}_3^0} \leq m_{\tilde{\chi}_4^0} \leq m_{\tilde{\chi}_5^0}$ .

- For the stop, sbottom and stau matrices, in the  $(\tilde{q}_L, \tilde{q}_R)$  basis, we have

$$\begin{aligned} \tilde{\mathcal{M}}_t^2 &= \begin{pmatrix} M_{\tilde{Q}_3}^2 + m_t^2 + \cos 2\beta M_Z^2 (\frac{1}{2} - \frac{2}{3}s_W^2) & \frac{h_t^* v_u}{\sqrt{2}} (|A_t| e^{-i(\theta+\phi_{A_t})} - \frac{|\lambda|v_S}{\sqrt{2}} e^{i\phi'_\lambda} \cot \beta) \\ \frac{h_t v_u}{\sqrt{2}} (|A_t| e^{i(\theta+\phi_{A_t})} - \frac{|\lambda|v_S}{\sqrt{2}} e^{-i\phi'_\lambda} \cot \beta) & M_{\tilde{U}_3}^2 + m_t^2 + \cos 2\beta M_Z^2 Q_t s_W^2 \end{pmatrix}, \\ \tilde{\mathcal{M}}_b^2 &= \begin{pmatrix} M_{\tilde{Q}_3}^2 + m_b^2 + \cos 2\beta M_Z^2 (-\frac{1}{2} + \frac{1}{3}s_W^2) & \frac{h_b^* v_d}{\sqrt{2}} (|A_b| e^{-i\phi_{A_b}} - \frac{|\lambda|v_S}{\sqrt{2}} e^{i\phi'_\lambda} \tan \beta) / \sqrt{2} \\ \frac{h_b v_d}{\sqrt{2}} (|A_b| e^{i\phi_{A_b}} - \frac{|\lambda|v_S}{\sqrt{2}} e^{-i\phi'_\lambda} \tan \beta) / \sqrt{2} & M_{\tilde{D}_3}^2 + m_b^2 + \cos 2\beta M_Z^2 Q_b s_W^2 \end{pmatrix}, \\ \tilde{\mathcal{M}}_\tau^2 &= \begin{pmatrix} M_{\tilde{L}_3}^2 + m_\tau^2 + \cos 2\beta M_Z^2 (s_W^2 - 1/2) & \frac{h_\tau^* v_d}{\sqrt{2}} (|A_\tau| e^{-i\phi_{A_\tau}} - \frac{|\lambda|v_S}{\sqrt{2}} e^{i\phi'_\lambda} \tan \beta) / \sqrt{2} \\ \frac{h_\tau v_d}{\sqrt{2}} (|A_\tau| e^{i\phi_{A_\tau}} - \frac{|\lambda|v_S}{\sqrt{2}} e^{-i\phi'_\lambda} \tan \beta) / \sqrt{2} & M_{\tilde{E}_3}^2 + m_\tau^2 - \cos 2\beta M_Z^2 s_W^2 \end{pmatrix}, \end{aligned} \quad (\text{A.3})$$

where  $h_\tau \equiv \frac{2m_\tau}{v_d}$  and  $m_\tau$  are the Yukawa coupling and mass of the  $\tau$  lepton, respectively, and  $A_\tau \equiv |A_\tau| e^{i\phi_{A_\tau}}$  is the soft Yukawa coupling of  $\tilde{\tau}$ . The mass eigenstates of the top and bottom squarks and the stau are obtained by diagonalising the above mass matrices as  $U^{\tilde{f}\dagger} \tilde{\mathcal{M}}_f^2 U^{\tilde{f}} = \text{diag}(m_{\tilde{f}_1}^2, m_{\tilde{f}_2}^2)$ , such that  $m_{\tilde{f}_1}^2 \leq m_{\tilde{f}_2}^2$ , for  $f = t, b$  and  $\tau$ .

## B Functions

- The functions used in the leading (s)quark corrections to the Higgs mass matrix are given as

$$\begin{aligned}
L_{\tilde{t}} &= \ln \left( \frac{m_{\tilde{t}_2}^2}{m_{\tilde{t}_1}^2} \right), \quad L_{\tilde{b}} = \ln \left( \frac{m_{\tilde{b}_2}^2}{m_{\tilde{b}_1}^2} \right), \\
L_{\tilde{t}\tilde{t}} &= \ln \left( \frac{m_{\tilde{t}_1} m_{\tilde{t}_2}}{m_{\tilde{t}}^2} \right), \quad L_{\tilde{b}\tilde{b}} = \ln \left( \frac{m_{\tilde{b}_1} m_{\tilde{b}_2}}{m_{\tilde{b}}^2} \right), \\
f_t &= \frac{1}{m_{\tilde{t}_2}^2 - m_{\tilde{t}_1}^2} \left[ m_{\tilde{t}_2}^2 \ln \left( \frac{m_{\tilde{t}_2}^2}{M_{\text{SUSY}}^2} \right) - m_{\tilde{t}_1}^2 \ln \left( \frac{m_{\tilde{t}_1}^2}{M_{\text{SUSY}}^2} \right) \right] - 1, \\
f_b &= \frac{1}{m_{\tilde{b}_2}^2 - m_{\tilde{b}_1}^2} \left[ m_{\tilde{b}_2}^2 \ln \left( \frac{m_{\tilde{b}_2}^2}{M_{\text{SUSY}}^2} \right) - m_{\tilde{b}_1}^2 \ln \left( \frac{m_{\tilde{b}_1}^2}{M_{\text{SUSY}}^2} \right) \right] - 1, \\
g_t &= \left[ \frac{m_{\tilde{t}_2}^2 + m_{\tilde{t}_1}^2}{m_{\tilde{t}_2}^2 - m_{\tilde{t}_1}^2} L_{\tilde{t}} - 2 \right], \quad g_b = \left[ \frac{m_{\tilde{b}_2}^2 + m_{\tilde{b}_1}^2}{m_{\tilde{b}_2}^2 - m_{\tilde{b}_1}^2} L_{\tilde{b}} - 2 \right],
\end{aligned} \tag{B.1}$$

where the mass eigenvalues  $m_{\tilde{q}}$  have been given in Appendix A.

- Additional quantities used in the  $D$ -term contributions are given as

$$\begin{aligned}
g_u &= \frac{1}{4}g_2^2 - \frac{5}{12}g_1^2, \quad g_d = \frac{1}{4}g_2^2 - \frac{1}{12}g_1^2, \\
D_u &= \frac{1}{2} \left( M_{\tilde{Q}_3} - M_{\tilde{U}_3} + \frac{g_u}{2}(v_d^2 - v_u^2) \right), \\
D_d &= \frac{1}{2} \left( M_{\tilde{Q}_3} - M_{\tilde{D}_3} + \frac{g_d}{2}(v_u^2 - v_d^2) \right), \\
C_t &= \frac{3m_t^2}{32\pi^2} \left[ \frac{4g_u D_u}{(m_{\tilde{t}_2}^2 - m_{\tilde{t}_1}^2)^2} g'_t - \frac{g_1^2 + g_2^2}{2(m_{\tilde{t}_2}^2 - m_{\tilde{t}_1}^2)} L_{\tilde{t}} \right], \\
C_b &= \frac{3m_b^2}{32\pi^2} \left[ \frac{4g_d D_d}{(m_{\tilde{b}_2}^2 - m_{\tilde{b}_1}^2)^2} g'_b - \frac{g_1^2 + g_2^2}{2(m_{\tilde{b}_2}^2 - m_{\tilde{b}_1}^2)} L_{\tilde{b}} \right], \\
D_t &= -\frac{3m_t^2}{16\pi^2} \left[ \frac{2g_u D_u}{(m_{\tilde{t}_2}^2 - m_{\tilde{t}_1}^2)} L_{\tilde{t}} + \frac{g_1^2 + g_2^2}{4} \ln \left( \frac{m_{\tilde{t}_1}^2 m_{\tilde{t}_2}^2}{M_{\text{SUSY}}^2} \right) \right], \\
D_b &= -\frac{3m_b^2}{16\pi^2} \left[ \frac{2g_d D_d}{(m_{\tilde{b}_2}^2 - m_{\tilde{b}_1}^2)} L_{\tilde{b}} + \frac{g_1^2 + g_2^2}{4} \ln \left( \frac{m_{\tilde{b}_1}^2 m_{\tilde{b}_2}^2}{M_{\text{SUSY}}^2} \right) \right].
\end{aligned} \tag{B.2}$$

- The chargino/neutralino corrections use the following potentially large logarithms:

$$\begin{aligned}
L_\mu &= \ln \left( \frac{|\mu|^2}{M_{\text{SUSY}}^2} \right), \quad L_\nu = \ln \left( \frac{4|\nu|^2}{M_{\text{SUSY}}^2} \right), \\
L_{M_2\mu} &= \ln \left( \frac{\max(M_{1,2}^2, |\mu|^2)}{M_{\text{SUSY}}^2} \right), \quad L_{\mu\nu} = \ln \left( \frac{\max(4|\nu|^2, |\mu|^2)}{M_{\text{SUSY}}^2} \right),
\end{aligned} \tag{B.3}$$

where for simplification we assume  $M_1 \sim M_2 \equiv M_{1,2}$  for the gaugino masses.

- The Higgs wave function renormalisation constants for the three weak eigenstates  $H_u$ ,  $H_d$  and  $S$  are given, in the Landau gauge, as

$$\begin{aligned}
Z_{H_u} &= 1 + \frac{1}{16\pi^2} \left[ 3h_t^2 \ln \left( \frac{M_{\text{SUSY}}^2}{m_t^2} \right) - \frac{3}{4}(g_1^2 + 3g_2^2) \ln \left( \frac{M_{\text{SUSY}}^2}{m_Z^2} \right) \right. \\
&\quad + \cos^2 \left( 3h_b^2 + h_\tau^2 - 3h_t^2 \right) \ln \left( \frac{M_A^2}{m_t^2} \right) + \frac{g_1^2}{2} \ln \left( \frac{M_{\text{SUSY}}^2}{\max(|\mu|^2, M_1^2)} \right) \\
&\quad \left. + \frac{3g_2^2}{2} \ln \left( \frac{M_{\text{SUSY}}^2}{\max(|\mu|^2, M_2^2)} \right) + \lambda^2 \ln \left( \frac{M_{\text{SUSY}}^2}{\max(|\mu|^2, 4|\nu|^2)} \right) \right], \\
Z_{H_d} &= 1 + \frac{1}{16\pi^2} \left[ (3h_b^2 + h_\tau^2) \ln \left( \frac{M_{\text{SUSY}}^2}{m_t^2} \right) - \frac{3}{4}(g_1^2 + 3g_2^2) \ln \left( \frac{M_{\text{SUSY}}^2}{m_Z^2} \right) \right. \\
&\quad + \sin^2 \left( 3h_t^2 - h_\tau^2 - 3h_b^2 \right) \ln \left( \frac{M_A^2}{m_t^2} \right) + \frac{g_1^2}{2} \ln \left( \frac{M_{\text{SUSY}}^2}{\max(|\mu|^2, M_1^2)} \right) \\
&\quad \left. + \frac{3g_2^2}{2} \ln \left( \frac{M_{\text{SUSY}}^2}{\max(|\mu|^2, M_2^2)} \right) + l^2 \ln \left( \frac{M_{\text{SUSY}}^2}{\max(|\mu|^2, 4|\nu|^2)} \right) \right], \\
Z_S &= 1 + \frac{1}{8\pi^2} \left[ \lambda^2 \ln \left( \frac{M_{\text{SUSY}}^2}{|\mu|^2} \right) + \kappa^2 \ln \left( \frac{M_{\text{SUSY}}^2}{4|\nu|^2} \right) \right]. \tag{B.4}
\end{aligned}$$

## References

- [1] **ATLAS Collaboration** Collaboration, G. Aad *et al.*, “Observation of a new particle in the search for the Standard Model Higgs boson with the ATLAS detector at the LHC,” *Phys.Lett.* **B716** (2012) 1–29, [arXiv:1207.7214 \[hep-ex\]](#).
- [2] **CMS Collaboration** Collaboration, S. Chatrchyan *et al.*, “Observation of a new boson at a mass of 125 GeV with the CMS experiment at the LHC,” *Phys.Lett.* **B716** (2012) 30–61, [arXiv:1207.7235 \[hep-ex\]](#).
- [3] S. Meola, “Measurements of properties of the Higgs-like Particle at 125 GeV by the CMS collaboration,” [arXiv:1310.4146 \[hep-ex\]](#).
- [4] <https://twiki.cern.ch/twiki/bin/view/CMSPublic/PhysicsResultsHIG>
- [5] <https://twiki.cern.ch/twiki/bin/view/AtlasPublic/HiggsPublicResults>
- [6] J. Christenson, J. Cronin, V. Fitch, and R. Turlay, “Evidence for the 2 pi Decay of the k(2)0 Meson,” *Phys.Rev.Lett.* **13** (1964) 138–140.
- [7] M. Kobayashi and T. Maskawa, “CP Violation in the Renormalizable Theory of Weak Interaction,” *Prog.Theor.Phys.* **49** (1973) 652–657.
- [8] T. Ibrahim and P. Nath, “CP Violation From Standard Model to Strings,” *Rev.Mod.Phys.* **80** (2008) 577–631, [arXiv:0705.2008 \[hep-ph\]](#).
- [9] A. Pilaftsis, “CP odd tadpole renormalization of Higgs scalar - pseudoscalar mixing,” *Phys.Rev.* **D58** (1998) 096010, [arXiv:hep-ph/9803297 \[hep-ph\]](#). ; A. Pilaftsis, “Higgs scalar - pseudoscalar mixing in the minimal supersymmetric standard model,” *Phys.Lett.* **B435** (1998) 88–100, [arXiv:hep-ph/9805373 \[hep-ph\]](#).



- [10] A. Pilaftsis and C. E. Wagner, “Higgs bosons in the minimal supersymmetric standard model with explicit CP violation,” *Nucl.Phys.* **B553** (1999) 3–42, [arXiv:hep-ph/9902371 \[hep-ph\]](#). ; M. S. Carena, J. R. Ellis, A. Pilaftsis, and C. Wagner, “Renormalization group improved effective potential for the MSSM Higgs sector with explicit CP violation,” *Nucl.Phys.* **B586** (2000) 92–140, [arXiv:hep-ph/0003180 \[hep-ph\]](#).
- [11] S. Choi, M. Drees, and J. S. Lee, “Loop corrections to the neutral Higgs boson sector of the MSSM with explicit CP violation,” *Phys.Lett.* **B481** (2000) 57–66, [arXiv:hep-ph/0002287 \[hep-ph\]](#). ; M. S. Carena, J. R. Ellis, A. Pilaftsis, and C. Wagner, “Higgs boson pole masses in the MSSM with explicit CP violation,” *Nucl.Phys.* **B625** (2002) 345–371, [arXiv:hep-ph/0111245 \[hep-ph\]](#). ; M. S. Carena, J. R. Ellis, S. Mrenna, A. Pilaftsis, and C. Wagner, “Collider probes of the MSSM Higgs sector with explicit CP violation,” *Nucl.Phys.* **B659** (2003) 145–178, [arXiv:hep-ph/0211467 \[hep-ph\]](#). ; S. Choi, J. Kalinowski, Y. Liao, and P. Zerwas, “H/A Higgs mixing in CP-noninvariant supersymmetric theories,” *Eur.Phys.J.* **C40** (2005) 555–564, [arXiv:hep-ph/0407347 \[hep-ph\]](#). ; M. Frank, T. Hahn, S. Heinemeyer, W. Hollik, H. Rzehak, *et al.*, “The Higgs Boson Masses and Mixings of the Complex MSSM in the Feynman-Diagrammatic Approach,” *JHEP* **0702** (2007) 047, [arXiv:hep-ph/0611326 \[hep-ph\]](#). ; S. Heinemeyer, W. Hollik, H. Rzehak, and G. Weiglein, “The Higgs sector of the complex MSSM at two-loop order: QCD contributions,” *Phys.Lett.* **B652** (2007) 300–309, [arXiv:0705.0746 \[hep-ph\]](#).
- [12] D. A. Demir, “Effects of the supersymmetric phases on the neutral Higgs sector,” *Phys.Rev.* **D60** (1999) 055006, [arXiv:hep-ph/9901389 \[hep-ph\]](#). ; G. L. Kane and L.-T. Wang, “Implications of supersymmetry phases for Higgs boson signals and limits,” *Phys.Lett.* **B488** (2000) 383–389, [arXiv:hep-ph/0003198 \[hep-ph\]](#). ; M. S. Carena, J. R. Ellis, A. Pilaftsis, and C. Wagner, “CP violating MSSM Higgs bosons in the light of LEP-2,” *Phys.Lett.* **B495** (2000) 155–163, [arXiv:hep-ph/0009212 \[hep-ph\]](#). ; A. Arhrib, D. K. Ghosh, and O. C. Kong, “Observing CP violating MSSM Higgs bosons at hadron colliders?,” *Phys.Lett.* **B537** (2002) 217–226, [arXiv:hep-ph/0112039 \[hep-ph\]](#). ; S. Choi, K. Hagiwara, and J. S. Lee, “Higgs boson decays in the minimal supersymmetric standard model with radiative Higgs sector CP violation,” *Phys.Rev.* **D64** (2001) 032004, [arXiv:hep-ph/0103294 \[hep-ph\]](#). ; S. Choi, M. Drees, J. S. Lee, and J. Song, “Supersymmetric Higgs boson decays in the MSSM with explicit CP violation,” *Eur.Phys.J.* **C25** (2002) 307–313, [arXiv:hep-ph/0204200 \[hep-ph\]](#). ; J. R. Ellis, J. S. Lee, and A. Pilaftsis, “Resonant CP violation in Higgs radiation at  $e^+e^-$  linear collider,” *Phys.Rev.* **D72** (2005) 095006, [arXiv:hep-ph/0507046 \[hep-ph\]](#). ; K. E. Williams, H. Rzehak, and G. Weiglein, “Higher order corrections to Higgs boson decays in the MSSM with complex parameters,” *Eur.Phys.J.* **C71** (2011) 1669, [arXiv:1103.1335 \[hep-ph\]](#). ; T. Fritzsche, S. Heinemeyer, H. Rzehak, and C. Schappacher, “Heavy Scalar Top Quark Decays in the Complex MSSM: A Full One-Loop Analysis,” *Phys.Rev.* **D86** (2012) 035014, [arXiv:1111.7289 \[hep-ph\]](#).
- [13] M. S. Carena, M. Quiros, and C. Wagner, “Opening the window for electroweak baryogenesis,” *Phys.Lett.* **B380** (1996) 81–91, [arXiv:hep-ph/9603420 \[hep-ph\]](#). ; M. S. Carena, M. Quiros, A. Riotto, I. Vilja, and C. Wagner, “Electroweak baryogenesis and low-energy supersymmetry,” *Nucl.Phys.* **B503** (1997) 387–404, [arXiv:hep-ph/9702409 \[hep-ph\]](#). ; M. S. Carena, J. Moreno, M. Quiros, M. Seco, and C. Wagner, “Supersymmetric CP violating currents and electroweak baryogenesis,” *Nucl.Phys.* **B599** (2001) 158–184, [arXiv:hep-ph/0011055 \[hep-ph\]](#). ; M. S. Carena, M. Quiros, M. Seco, and C. Wagner, “Im-



- proved results in supersymmetric electroweak baryogenesis,” *Nucl.Phys.* **B650** (2003) 24–42, [arXiv:hep-ph/0208043 \[hep-ph\]](#). ; M. Carena, G. Nardini, M. Quiros, and C. Wagner, “The Baryogenesis Window in the MSSM,” *Nucl.Phys.* **B812** (2009) 243–263, [arXiv:0809.3760 \[hep-ph\]](#). ; V. Cirigliano, Y. Li, S. Profumo, and M. J. Ramsey-Musolf, “MSSM Baryogenesis and Electric Dipole Moments: An Update on the Phenomenology,” *JHEP* **1001** (2010) 002, [arXiv:0910.4589 \[hep-ph\]](#). ; M. Carena, G. Nardini, M. Quiros, and C. E. Wagner, “MSSM Electroweak Baryogenesis and LHC Data,” *JHEP* **1302** (2013) 001, [arXiv:1207.6330 \[hep-ph\]](#).
- [14] C. Baker, D. Doyle, P. Geltenbort, K. Green, M. van der Grinten, *et al.*, “An Improved experimental limit on the electric dipole moment of the neutron,” *Phys.Rev.Lett.* **97** (2006) 131801, [arXiv:hep-ex/0602020 \[hep-ex\]](#). ; E. D. Commins, “Electric dipole moments of elementary particles, nuclei, atoms, and molecules,” *J.Phys.Soc.Jap.* **76** (2007) 111010. ; W. Griffith, M. Swallows, T. Loftus, M. Romalis, B. Heckel, *et al.*, “Improved Limit on the Permanent Electric Dipole Moment of Hg-199,” *Phys.Rev.Lett.* **102** (2009) 101601.
- [15] A. Dedes and S. Moretti, “Effect of large supersymmetric phases on Higgs production,” *Phys.Rev.Lett.* **84** (2000) 22–25, [arXiv:hep-ph/9908516 \[hep-ph\]](#). ; A. Dedes and S. Moretti, “Effects of CP violating phases on Higgs boson production at hadron colliders in the minimal supersymmetric standard model,” *Nucl.Phys.* **B576** (2000) 29–55, [arXiv:hep-ph/9909418 \[hep-ph\]](#). ; S. Choi, K. Hagiwara, and J. S. Lee, “Observability of the lightest MSSM Higgs boson with explicit CP violation via gluon fusion at the LHC,” *Phys.Lett.* **B529** (2002) 212–221, [arXiv:hep-ph/0110138 \[hep-ph\]](#). ; J. R. Ellis, J. S. Lee, and A. Pilaftsis, “CERN LHC signatures of resonant CP violation in a minimal supersymmetric Higgs sector,” *Phys.Rev.* **D70** (2004) 075010, [arXiv:hep-ph/0404167 \[hep-ph\]](#). ; S. Moretti, S. Munir, and P. Poulose, “Explicit CP Violation in the MSSM Through  $Higgs \rightarrow \gamma\gamma$ ,” *Phys.Lett.* **B649** (2007) 206–211, [arXiv:hep-ph/0702242 \[HEP-PH\]](#). ; S. Hesselbach, S. Moretti, S. Munir, and P. Poulose, “Exploring the Di-Photon Decay of a Light Higgs Boson in the MSSM With Explicit CP Violation,” *Eur.Phys.J.* **C54** (2008) 129–147, [arXiv:0706.4269 \[hep-ph\]](#). ; S. Hesselbach, S. Moretti, S. Munir, and P. Poulose, “Explicit CP violation in the MSSM through  $gg \rightarrow H \rightarrow \gamma\gamma$ ,” *Phys.Rev.* **D82** (2010) 074004, [arXiv:0903.0747 \[hep-ph\]](#).
- [16] A. Chakraborty, B. Das, J. L. Diaz-Cruz, D. K. Ghosh, S. Moretti, *et al.*, “The 125 GeV Higgs signal at the LHC in the CP Violating MSSM,” [arXiv:1301.2745 \[hep-ph\]](#).
- [17] P. Fayet, “Supergauge Invariant Extension of the Higgs Mechanism and a Model for the electron and Its Neutrino,” *Nucl.Phys.* **B90** (1975) 104–124. ; J. R. Ellis, J. Gunion, H. E. Haber, L. Roszkowski, and F. Zwirner, “Higgs Bosons in a Nonminimal Supersymmetric Model,” *Phys.Rev.* **D39** (1989) 844.
- [18] L. Durand and J. L. Lopez, “Upper Bounds on Higgs and Top Quark Masses in the Flipped  $SU(5) \times U(1)$  Superstring Model,” *Phys.Lett.* **B217** (1989) 463. ; M. Drees, “Supersymmetric Models with Extended Higgs Sector,” *Int.J.Mod.Phys.* **A4** (1989) 3635.
- [19] D. Miller, R. Nevzorov, and P. Zerwas, “The Higgs sector of the next-to-minimal supersymmetric standard model,” *Nucl.Phys.* **B681** (2004) 3–30, [arXiv:hep-ph/0304049 \[hep-ph\]](#).
- [20] U. Ellwanger, C. Hugonie, and A. M. Teixeira, “The Next-to-Minimal Supersymmetric Standard Model,” *Phys.Rept.* **496** (2010) 1–77, [arXiv:0910.1785 \[hep-ph\]](#).

- [21] M. Maniatis, “The Next-to-Minimal Supersymmetric extension of the Standard Model reviewed,” *Int.J.Mod.Phys.* **A25** (2010) 3505–3602, [arXiv:0906.0777 \[hep-ph\]](#).
- [22] U. Ellwanger, “A Higgs boson near 125 GeV with enhanced di-photon signal in the NMSSM,” *JHEP* **1203** (2012) 044, [arXiv:1112.3548 \[hep-ph\]](#).
- [23] J. F. Gunion, Y. Jiang, and S. Kraml, “Could two NMSSM Higgs bosons be present near 125 GeV?,” *Phys.Rev.* **D86** (2012) 071702, [arXiv:1207.1545 \[hep-ph\]](#).
- [24] S. Munir, L. Roszkowski, and S. Trojanowski, “Simultaneous enhancement in  $\gamma\gamma$ ,  $b\bar{b}$  and  $\tau^+\tau^-$  rates in the NMSSM with nearly degenerate scalar and pseudoscalar Higgs bosons,” *Phys. Rev.* **D88** (2013) 055017, [arXiv:1305.0591 \[hep-ph\]](#).
- [25] B. Ananthanarayan, J. Lahiri, P. Pandita, and M. Patra, “Invisible decays of the lightest Higgs boson in supersymmetric models,” *Phys.Rev.* **D87** (2013) 115021, [arXiv:1306.1291 \[hep-ph\]](#).
- [26] J. Cao, F. Ding, C. Han, J. M. Yang, and J. Zhu, “A light Higgs scalar in the NMSSM confronted with the latest LHC Higgs data,” *JHEP* **1311** (2013) 018, [arXiv:1309.4939 \[hep-ph\]](#).
- [27] S. Moretti, S. Munir, and P. Poulose, “125 GeV Higgs Boson signal within the complex NMSSM,” *Phys.Rev.* **D89** (2014) 015022, [arXiv:1305.0166 \[hep-ph\]](#).
- [28] S. Abel, S. Khalil, and O. Lebedev, “EDM constraints in supersymmetric theories,” *Nucl.Phys.* **B606** (2001) 151–182, [arXiv:hep-ph/0103320 \[hep-ph\]](#).
- [29] N. Haba, “Explicit CP violation in the Higgs sector of the next-to-minimal supersymmetric standard model,” *Prog.Theor.Phys.* **97** (1997) 301–310, [arXiv:hep-ph/9608357 \[hep-ph\]](#). ; T. Ibrahim and P. Nath, “The Neutron and the lepton EDMs in MSSM, large CP violating phases, and the cancellation mechanism,” *Phys.Rev.* **D58** (1998) 111301, [arXiv:hep-ph/9807501 \[hep-ph\]](#). ; M. Boz, “The Higgs sector and electron electric dipole moment in next-to-minimal supersymmetry with explicit CP violation,” *Mod.Phys.Lett.* **A21** (2006) 243–264, [arXiv:hep-ph/0511072 \[hep-ph\]](#). ; J. R. Ellis, J. S. Lee, and A. Pilaftsis, “Electric Dipole Moments in the MSSM Reloaded,” *JHEP* **0810** (2008) 049, [arXiv:0808.1819 \[hep-ph\]](#). ; Y. Li, S. Profumo, and M. Ramsey-Musolf, “A Comprehensive Analysis of Electric Dipole Moment Constraints on CP-violating Phases in the MSSM,” *JHEP* **1008** (2010) 062, [arXiv:1006.1440 \[hep-ph\]](#).
- [30] T. Graf, R. Grober, M. Muhlleitner, H. Rzehak, and K. Walz, “Higgs Boson Masses in the Complex NMSSM at One-Loop Level,” *JHEP* **1210** (2012) 122, [arXiv:1206.6806 \[hep-ph\]](#).
- [31] S. Ham, S. Oh, and D. Son, “Neutral Higgs sector of the next-to-minimal supersymmetric standard model with explicit CP violation,” *Phys.Rev.* **D65** (2002) 075004, [arXiv:hep-ph/0110052 \[hep-ph\]](#). ; K. Funakubo and S. Tao, “The Higgs sector in the next-to-MSSM,” *Prog.Theor.Phys.* **113** (2005) 821–842, [arXiv:hep-ph/0409294 \[hep-ph\]](#).
- [32] K. Cheung, T.-J. Hou, J. S. Lee, and E. Senaha, “The Higgs Boson Sector of the Next-to-MSSM with CP Violation,” *Phys.Rev.* **D82** (2010) 075007, [arXiv:1006.1458 \[hep-ph\]](#). ; K. Cheung, T.-J. Hou, J. S. Lee, and E. Senaha, “Higgs Mediated EDMs in the Next-to-MSSM: An Application to Electroweak Baryogenesis,” *Phys.Rev.* **D84** (2011) 015002, [arXiv:1102.5679 \[hep-ph\]](#).

- [33] <http://www.th.u-psud.fr/NMHDECAY/nmssmtools.html>
- [34] J. Lee, A. Pilaftsis, M. S. Carena, S. Choi, M. Drees, *et al.*, “CPsuperH: A Computational tool for Higgs phenomenology in the minimal supersymmetric standard model with explicit CP violation,” *Comput.Phys.Commun.* **156** (2004) 283–317, [arXiv:hep-ph/0307377](#) [hep-ph].
- [35] M. Spira, “QCD effects in Higgs physics,” *Fortsch.Phys.* **46** (1998) 203–284, [arXiv:hep-ph/9705337](#) [hep-ph].
- [36] M. Spira, A. Djouadi, D. Graudenz, and P. Zerwas, “Higgs boson production at the LHC,” *Nucl.Phys.* **B453** (1995) 17–82, [arXiv:hep-ph/9504378](#) [hep-ph].
- [37] G. Degrandi and P. Slavich, “On the radiative corrections to the neutral Higgs boson masses in the NMSSM,” *Nucl.Phys.* **B825** (2010) 119–150, [arXiv:0907.4682](#) [hep-ph].
- [38] S. King, M. Muhlleitner, and R. Nevzorov, “NMSSM Higgs Benchmarks Near 125 GeV,” *Nucl.Phys.* **B860** (2012) 207–244, [arXiv:1201.2671](#) [hep-ph]. ; J. F. Gunion, Y. Jiang, and S. Kraml, “The Constrained NMSSM and Higgs near 125 GeV,” *Phys.Lett.* **B710** (2012) 454–459, [arXiv:1201.0982](#) [hep-ph]. ; R. Benbrik, M. Gomez Bock, S. Heinemeyer, O. Stal, G. Weiglein, *et al.*, “Confronting the MSSM and the NMSSM with the Discovery of a Signal in the two Photon Channel at the LHC,” *Eur.Phys.J.* **C72** (2012) 2171, [arXiv:1207.1096](#) [hep-ph]. ; S. King, M. Muhlleitner, R. Nevzorov, and K. Walz, “Natural NMSSM Higgs Bosons,” *Nucl.Phys.* **B870** (2013) 323–352, [arXiv:1211.5074](#) [hep-ph]. ; K. Kowalska, S. Munir, L. Roszkowski, E. M. Sessolo, S. Trojanowski, *et al.*, “The Constrained NMSSM with a 125 GeV Higgs boson – A global analysis,” *Phys. Rev.* **D87** (2013) 115010, [arXiv:1211.1693](#) [hep-ph]. ; T. Gherghetta, B. von Harling, A. D. Medina, and M. A. Schmidt, “The Scale-Invariant NMSSM and the 126 GeV Higgs Boson,” *JHEP* **1302** (2013) 032, [arXiv:1212.5243](#) [hep-ph]. ; R. Barbieri, D. Buttazzo, K. Kannike, F. Sala, and A. Tesi, “Exploring the Higgs sector of a most natural NMSSM,” *Phys. Rev. D* **87**, **115018** (2013) , [arXiv:1304.3670](#) [hep-ph].
- [39] U. Ellwanger and C. Hugonie, “Higgs bosons near 125 GeV in the NMSSM with constraints at the GUT scale,” *Adv.High Energy Phys.* **2012** (2012) 1, [arXiv:1203.5048](#) [hep-ph].
- [40] U. Ellwanger, “Higgs pair production in the NMSSM at the LHC,” *JHEP* **1308** (2013) 077, [arXiv:1306.5541](#) [hep-ph].
- [41] “Evidence for higgs boson decays to the  $\tau^+\tau$  final state with the atlas detector,” Tech. Rep. ATLAS-CONF-2013-108, CERN, Geneva, Nov, 2013
- [42] “Search for the standard-model higgs boson decaying to tau pairs in proton-proton collisions at  $\sqrt{s} = 7$  and 8 tev,” Tech. Rep. CMS-PAS-HIG-13-004, CERN, Geneva, 2013
- [43] M. Badziak, M. Olechowski, and S. Pokorski, “New Regions in the NMSSM with a 125 GeV Higgs,” *JHEP* **1306** (2013) 043, [arXiv:1304.5437](#) [hep-ph].
- [44] “Inclusive search for doubly charged higgs in leptonic final states with the 2011 data at 7 tev,” Tech. Rep. CMS-PAS-HIG-13-005, CERN, Geneva, 2013
- [45] “Combined coupling measurements of the higgs-like boson with the atlas detector using up to 25 fb $^{-1}$  of proton-proton collision data,” Tech. Rep. ATLAS-CONF-2013-034, CERN, Geneva, Mar, 2013

- [46] **LEP Working Group for Higgs boson searches, ALEPH Collaboration, DELPHI Collaboration, L3 Collaboration, OPAL Collaboration** Collaboration, R. Barate *et al.*, “Search for the standard model Higgs boson at LEP,” *Phys.Lett.* **B565** (2003) 61–75, [arXiv:hep-ex/0306033](#) [hep-ex].
- [47] **XENON100 Collaboration** Collaboration, E. Aprile *et al.*, “Dark Matter Results from 225 Live Days of XENON100 Data,” *Phys.Rev.Lett.* **109** (2012) 181301, [arXiv:1207.5988](#) [astro-ph.CO].
- [48] Z. Kang, J. Li, T. Li, D. Liu, and J. Shu, “Probing the CP-even Higgs Sector via  $H_3 \rightarrow H_2 H_1$  in the Natural NMSSM,” *Phys.Rev.* **D88** (2013) 015006, [arXiv:1301.0453](#) [hep-ph].
- [49] D. T. Nhung, M. Muhlleitner, J. Streicher, and K. Walz, “Higher Order Corrections to the Trilinear Higgs Self-Couplings in the Real NMSSM,” [arXiv:1306.3926](#) [hep-ph].
- [50] J. M. No and M. Ramsey-Musolf, “Probing the Higgs Portal at the LHC Through Resonant di-Higgs Production,” [arXiv:1310.6035](#) [hep-ph].
- [51] A. Belyaev, N. D. Christensen, and A. Pukhov, “CalcHEP 3.4 for collider physics within and beyond the Standard Model,” *Comput.Phys.Commun.* **184** (2013) 1729–1769, [arXiv:1207.6082](#) [hep-ph].